universe

MDPI

Article

Study of Singly Charmed Dibaryons in Quark Model

Yuxuan Du [1], Yao Cui [1], Zhiyun Tan [2], Jin Tao [1,*], Hongxia Huang [1,*] and Jialun Ping [1]

[1] Department of Physics, Nanjing Normal University, Nanjing 210097, China; 241002008@njnu.edu.cn (Y.D.); 221002055@njnu.edu.cn (Y.C.); jlping@njnu.edu.cn (J.P.)
[2] School of Physics and Electronic Science, Zunyi Normal College, Zunyi 563006, China; zytan@zync.edu.cn
* Correspondence: 06198@njnu.edu.cn (J.T.); hxhuang@njnu.edu.cn (H.H.)

Abstract

We perform a systematic investigation of low-lying singly charmed dibaryon systems with $J = 1, I = 0, \frac{1}{2}, 1, \frac{3}{2}, 2, \frac{5}{2}$ and strangeness $S = -1, -2, -3, -4, -5$ in the chiral quark model. According to the analysis of effective potentials, dibaryon systems characterized by lower isospin and magnitude of strangeness exhibit stronger attractive interactions, which may enhance their tendency to form bound states. Experimental efforts may therefore prioritize the search for such configurations. The bound-state calculation results indicate that we have obtained some single-channel bound states, which are $\Sigma\Sigma_c$, $\Sigma\Sigma_c^*$, $\Sigma^*\Sigma_c$, $\Sigma^*\Sigma_c^*$ with $I = 0$, $S = -1$; $\Sigma_c\Delta$, $\Sigma_c^*\Delta$ with $I = \frac{1}{2}$, $S = 0$; $\Sigma\Sigma_c$ with $I = 1$, $S = -1$; $\Sigma_c\Delta$ with $I = \frac{3}{2}$, $S = 0$; and $\Xi^*\Sigma_c^*$ with $I = \frac{3}{2}$, $S = -2$. However, these states can decay through open channels. We have listed both these single-channel bound states and their corresponding decay channels in this work for experimental reference and search. In the future, we need to study the scattering processes of the open channels further to confirm whether these states are resonance states.

Keywords: singly charmed dibaryons; effective potentials; bound states; chrial quark model

1. Introduction

Research on dibaryon states has been conducted for many years. The earliest established dibaryon state, dating back to 1932, is the deuteron [1]. In 1977, based on the MIT bag model, Jaffe utilized gluon exchange interactions and discovered a stabilized configuration of six quarks, thereby predicting the existence of the H-dibaryon [2]. Over the past decade, researchers have persistently pursued the search for new dibaryon states, and the discovery of the dibaryon resonance d^* has undoubtedly inspired confidence among many scientists and physicists [3–5]. Beyond the H-dibaryon, the $N\Omega$ configuration has emerged in recent research as a prominently studied dibaryon system involving a strange quark. In 1987, T. Goldman proposed in two different quark models that a dibaryon state with the strangeness $S = -3$ might exist [6]. Numerous studies have been dedicated to this state over many years [7–10]. Recent theoretical studies have provided substantial evidence for the existence of the $N\Omega$ state [11,12]. In 2019, the STAR collaboration investigated the $N\Omega$ correlation function via relativistic heavy ion collisions in $Au + Au$ collisions, providing supporting evidence for the existence of $N\Omega$ [13]. Recently, the ALICE collaboration has investigated interactions between baryons containing strange quarks, specifically demonstrating the use of $N\Omega$ correlation functions for precision calculations [14]. Inspired by these findings, our group further investigated the $p - \Omega$ system from the perspective of the quark model, including the energy spectrum, scattering phase shifts, and correlation functions, and the results supported the existence of the $p - \Omega$ bound state [15].

check for updates

Academic Editor: Benjamin Grinstein

Received: 26 August 2025
Revised: 26 September 2025
Accepted: 16 October 2025
Published: 20 October 2025

Citation: Du, Y.; Cui, Y.; Tan, Z.; Tao, J.; Huang, H.; Ping, J. Study of Singly Charmed Dibaryons in Quark Model. *Universe* **2025**, *11*, 351. https://doi.org/10.3390/universe11100351

The experimental discovery of the doubly charmed baryon Ξ_{cc} by the LHCb Collaboration has further stimulated research into charmed baryons [16]. Moreover, the discovery of heavy baryons has also sparked significant interest among physicists in studying dibaryon states involving heavy quarks. Theoretically, the substantial mass of heavy quarks suppresses the kinetic term in the Hamiltonian, thereby enhancing the likelihood of bound-state formation. Consequently, a significant number of researchers have shifted their focus to the systematic search for charmed dibaryon states. Various theoretical approaches have focused on predicting the existence of heavy-flavor dibaryons. Some theoretical studies have employed the one-boson exchange model to investigate dibaryon states involving heavy quarks [17–21], N. Lee et al. performed a systematic study of the possible loosely bound states composed of two charmed baryons or a charmed baryon and an anti-charmed baryon. Their results indicate that the H-dibaryon-like state $\Lambda_c\Lambda_c$ does not exist, but deuteron-like states $\Xi_c\Xi_c$ and $\Xi_c'\Xi_c'$ may exist. In Ref. [21], Y. W. Pan et al. employed the one-boson exchange model to study the interactions between Ξ_{cc}^* and Σ_c^*, showing that several possible three-charm deuteron-like hexaquark states may exist. Some theoretical studies employed lattice quantum chromodynamics (QCD) sum rules to investigate dibaryon states with heavy flavor. In Ref. [22], Z. G. Wang constructed color-singlet-type currents to study scalar and axialvector Ξ_{cc} Σ_c^* dibaryon states with QCD sum rules. Some theoretical studies have utilized lattice QCD to investigate heavy dibaryon states [23–25]. In Ref. [23], P. Junnarkar et al. reported the first lattice QCD study of deuteron-like dibaryons with heavy quark flavors and found that the ground-state mass of dibaryon $\Omega_c\Omega_{cc}$ was below the two-baryon threshold and also predicted the mass precisely. In addition, some theoretical groups investigated heavy dibaryons within the framework of the quark model [26–30]. The work of Ref. [28] investigated doubly heavy dibaryon systems with strangeness $S = 0$ in the quark delocalization color screening model (QDCSM), and several bound systems were obtained. In Ref. [30], Y. Cui et al. performed a systematic investigation of the singly charmed deuteron-like dibaryon states ($IJ = 01$), and several resonance states were obtained. $\Sigma\Sigma_c$ appears as a resonance state in the $\Lambda\Lambda_c$ and $N\Xi_c^*$ scattering process, and $\Sigma\Sigma_c^*$ exhibits a resonance state in the $N\Xi_c$ and $N\Xi_c'$ scattering phase shifts. To explore more dibaryon states, it is meaningful and necessary to systematically search for dibaryon systems from light flavor to heavy flavor with all possible quantum numbers.

This paper focuses on the study of dibaryon states containing a singly charmed quark, with strangeness $S = -1,\ -2,\ -3, -4$, and -5, angular momentum quantum number $J = 1$, and isospin $I = 0,\ \frac{1}{2},\ 1,\ \frac{3}{2},\ 2,\ \frac{5}{2}$. The structure of this paper is organized as follows: Section 2 provides a concise introduction to the quark model and the resonating group method (RGM). Section 3 presents the numerical results and corresponding discussion. The final Section 4 delivers the conclusion.

2. Quark Model and Resonating Group Method

This work is conducted within the framework of the chiral quark model (ChQM), using the resonating group method (RGM) to search for dibaryon bound states containing charm quarks. This chapter will provide a brief introduction to the model and the method.

2.1. The Chiral Quark Model

The chiral quark model is one of the most common approaches to describe hadron spectra, hadron–hadron interactions, and multiquark states [31]. In this model, the short-range interaction is primarily provided by the one-gluon exchange potential, the intermediate range attraction is generated by the meson exchange potential, while the Goldstone boson exchange potential dominates the long-range interaction. Our study focuses on dibaryons with strange and charm quarks, necessitating an extension from SU(3) to SU(4) flavor sym-

metry. Within this expanded framework, the standard Goldstone boson exchange potential is no longer sufficient; we have incorporated the following meson exchange potentials: D-meson exchange potential between u/d and c quarks, D_s-meson exchange potential between s and c quarks, and η_c-meson exchange potential between any two quarks (u/d, s, or c quarks). Here, we only show the Hamiltonian and the parameters used.

$$H = \sum_{i=1}^{6}\left(m_i + \frac{p_i^2}{2m_i}\right) - T_c + \sum_{i<j} V_{ij} \tag{1}$$

$$V_{ij} = V^{\mathrm{CON}}(r_{ij}) + V^{\mathrm{OGE}}(r_{ij}) + V^{\sigma}(r_{ij}) + V^{\mathrm{OBE}}(r_{ij}) \tag{2}$$

where m_i is the mass of different quarks, the kinetic energy term in the Hamiltonian is $\frac{p_i^2}{2m_i}$, and the term for the kinetic energy of the center of mass is T_c. The potential interaction V_{ij} includes the confinement potential $V^{\mathrm{CON}}(r_{ij})$, the one-gluon exchange potential $V^{\mathrm{OGE}}(r_{ij})$, the σ meson exchange potential $V^{\sigma}(r_{ij})$, and the one-boson exchange potential $V^{\mathrm{OBE}}(r_{ij})$. Since this study only involves calculations for the ground state, we will only present the form of the central force here:

$$V^{\mathrm{CON}}(r_{ij}) = -a_c \boldsymbol{\lambda_i} \cdot \boldsymbol{\lambda_j}\left[r_{ij}^2 + V_0\right] \tag{3}$$

Additionally, based on the asymptotic freedom property of QCD, the model introduces the one-gluon exchange potential:

$$\begin{aligned} V^{\mathrm{OGE}}(r_{ij}) = \frac{1}{4}\alpha_{s_{q_iq_j}} \boldsymbol{\lambda_i} \cdot \boldsymbol{\lambda_j} \Bigg[& \frac{1}{r_{ij}} - \frac{\pi}{2} \\ & \left(\frac{1}{m_i^2} + \frac{1}{m_j^2} + \frac{4\boldsymbol{\sigma}_i \cdot \boldsymbol{\sigma}_j}{3m_i m_j}\right) \quad - \frac{3}{4m_i m_j r_{ij}^3} S_{ij} \Bigg] \end{aligned} \tag{4}$$

where S_{ij} is the quark tensor operator. We consider only $S-$wave states in this work; the tensor force operator does not contribute. In the chiral quark model, we introduce the scalar σ meson exchange potential (only between u and d quarks) to provide intermediate range attraction. Its specific expression is

$$V^{\sigma}(r_{ij}) = -\frac{g_{\mathrm{ch}}^2}{4\pi}\frac{\Lambda_\sigma^2 m_\sigma}{\Lambda_\sigma^2 - m_\sigma^2}\left[Y(m_\sigma r_{ij}) - \frac{\Lambda_\sigma}{m_\sigma} Y(\Lambda_\sigma r_{ij})\right] \tag{5}$$

For the Goldstone boson exchange potential $V^{\mathrm{OBE}}(r_{ij})$ arising from spontaneous chiral symmetry breaking, the specific expressions for each term are

$$\begin{aligned} V^{\mathrm{OBE}}(r_{ij}) = {} & \nu_\pi(r_{ij}) \sum_{a=1}^{3} \lambda_i^a \cdot \lambda_j^a + \nu_K(r_{ij}) \sum_{a=4}^{7} \lambda_i^a \cdot \lambda_j^a \\ & + \nu_\eta(r_{ij})\left[\left(\lambda_i^8 \cdot \lambda_j^8\right)\sin\theta_p - \left(\lambda_i^0 \cdot \lambda_j^0\right)\cos\theta_p\right] \\ & + \nu_D(r_{ij}) \sum_{a=9}^{12} \lambda_i^a \cdot \lambda_j^a + \nu_{D_s}(r_{ij}) \sum_{a=13}^{14} \lambda_i^a \cdot \lambda_j^a \\ & + \nu_{\eta_c}(r_{ij}) \lambda_i^{15} \cdot \lambda_j^{15} \end{aligned} \tag{6}$$

$$v_\chi(r_{ij}) = -\frac{g_{\rm ch}^2}{4\pi}\frac{m_\chi^2}{12m_im_j}\frac{\Lambda_\chi^2}{\Lambda_\chi^2 - m_\chi^2}m_\chi\Bigg\{ \left[Y(m_\chi r_{ij}) - \frac{\Lambda_\chi^3}{m_\chi^3}Y(\Lambda_\chi r_{ij})\right]\boldsymbol{\sigma}_i\cdot\boldsymbol{\sigma}_j + \left[H(m_\chi r_{ij}) - \frac{\Lambda_\chi^3}{m_\chi^3}H(\Lambda_\chi r_{ij})\right]S_{ij}\Bigg\} \quad (7)$$

$$S_{ij} = \frac{(\boldsymbol{\sigma}_i\cdot\boldsymbol{r}_{ij})(\boldsymbol{\sigma}_j\cdot\boldsymbol{r}_{ij})}{r_{ij}^2} - \frac{1}{3}\boldsymbol{\sigma}_i\cdot\boldsymbol{\sigma}_j \quad (8)$$

where $Y(x)$ and $H(x)$ are standard Yukawa functions [31]. The model parameters are determined as follows. The mass parameters (e.g., m_π, m_K, m_η, m_D, m_η, m_{D_s}, and m_{η_c}) take their experimental values. The mass of u/d-quark ($m_{u,d}$), cutoff parameters (e.g., Λ_π, Λ_K, and Λ_η), and the mixing angle θ_P are empirically fit [32]. The chiral coupling constant g_{ch} can be obtained from the πNN coupling constant through

$$\frac{g_{ch}^2}{4\pi} = \left(\frac{3}{5}\right)^2\frac{g_{\pi NN}^2}{4\pi}\frac{m_{u,d}^2}{m_N^2}. \quad (9)$$

The other adjustable parameters can be determined by fitting the ground-state light baryons and singly heavy baryons, and the MINUIT program is employed for the fitting. In quark model calculations, equivalent coupling constants are used to describe the spectra of baryons and mesons. As shown in $V^{\rm OGE}$, the chromomagnetic term is related to $\frac{\alpha_{s_{q_iq_j}}}{m_im_j}$, where $\alpha_{s_{q_iq_j}}$ is associated with the quark flavor and determined by the mass difference between two baryons with spins $S=\frac{1}{2}$, $S=\frac{3}{2}$, respectively. The mass of heavy quarks is relatively large, which reduces the mass difference between the two baryons with spins $S=\frac{1}{2}$, $S=\frac{3}{2}$. Therefore, it is necessary to increase the value of $\alpha_{s_{q_iq_j}}$ to counteract the influence of quark mass and obtain a mass difference more consistent with experimental values. Thus, a phenomenon occurs where $\alpha_{s_{uu}}$ is less than $\alpha_{s_{cc}}$. However, when considering quark mass, $\frac{\alpha_{s_{uu}}}{m_im_j}$ remains greater than $\frac{\alpha_{s_{cc}}}{m_im_j}$. The model parameters and the masses of the fitted baryons with errors are shown in Tables 1 and 2, respectively. The energies listed in Tables 1 and 2 are expressed in the natural unit system ($\hbar = c = 1$). Tables 1 and 2 show that the uncertainties of the parameters are very small, so the error of the calculated baryon spectrum is also small.

Table 2 shows that the influence of parameter errors on baryon spectra is minimal.

Table 1. Model parameters.

	$b\ (fm)$	$m_{u,d}$ (MeV)	m_s (MeV)
ChQM	$0.52088 \pm 0.57\times10^{-7}$	313	590 ± 0.09
	m_c (MeV)	a_c (MeVfm^{-2})	$V_0\ (fm^2)$
ChQM	1700 ± 0.10	49.560 ± 0.11	$-1.0778 \pm 0.67\times10^{-3}$
	$\alpha_{s_{qq}}$	$\alpha_{s_{qs}}$	$\alpha_{s_{ss}}$
ChQM	$0.67249 \pm 0.14\times10^{-2}$	$0.83964 \pm 0.13\times10^{-2}$	$0.71678 \pm 0.17\times10^{-2}$
	$\alpha_{s_{qc}}$	$\alpha_{s_{sc}}$	$\alpha_{s_{cc}}$
ChQM	$0.59298 \pm 0.13\times10^{-2}$	$0.60778 \pm 0.15\times10^{-2}$	$1.0810 \pm 0.50\times10^{-2}$

2.2. The Resonating Group Method

The resonating group method (RGM) represents one of the most common approximation approaches for nuclear physics problems. When extending this method to six-quark systems, the primary approximation in RGM involves assuming unchanged internal wave

functions of the constituent baryons while focusing solely on the relative motion wave function between the two baryons. This approximation effectively reduces the complex six-body problem to a simpler two-body problem. The only quantity that needs to be solved is the relative motion wave function of the two baryons.

$$\Psi_{6q} = \mathcal{A}\Big[[\phi_{B_1}(\boldsymbol{\rho_1}, \boldsymbol{\lambda_1})\phi_{B_2}(\boldsymbol{\rho_2}, \boldsymbol{\lambda_2})]^{[\sigma]IS}\chi(\boldsymbol{R})Z(\boldsymbol{R_c})\Big]^J \tag{10}$$

where the symbol $\mathcal{A}$ is the antisymmetrization operator. With the $SU(4)$ extension, both the light and heavy quarks are considered as identical particles. So, the symbol $\mathcal{A}$ is written as $\mathcal{A} = 1 - 9P_{36}$. The internal wave functions of the two three-quark clusters is ϕ_{B_i}; both $\boldsymbol{\rho_i}$ and $\boldsymbol{\lambda_i}$ are internal coordinates. The relative motion wave function between the two clusters is $\chi(\boldsymbol{R})$, in which $\boldsymbol{R}$ refers to the relative coordinate between the two clusters. $Z(\boldsymbol{R_c})$ denotes the center of mass motion wave function of the two clusters, where $\boldsymbol{R_c}$ represents the center-of-mass coordinate. In Formula (10), $\sigma = [222]$ provides the total color symmetry, I represents isospin quantum number, and S refers to the spin quantum number. We assume that the three-quark cluster wave function ϕ_{B_i} is the product of the harmonic oscillator ground-state wave function and the isospin–spin wave function $\eta_{I_iS_i}(B_i)$ and color wave function χ_{c_i}, expressed as

Table 2. The calculated masses (in MeV) of the baryons in ChQM. Experimental values (Exp) are taken from the Particle Data Group (PDG) [33].

	$\boldsymbol{N}$	$\boldsymbol{\Delta}$	$\boldsymbol{\Lambda}$	$\boldsymbol{\Sigma}$
ChQM	932.7 ± 0.975	1254.03 ± 0.561	1104.85 ± 1.018	1207.94 ± 0.878
Exp	939	1233	1116	1189
	Σ^*	Ω	Ξ	Ξ^*
ChQM	1374.63 ± 0.675	1662.98 ± 0.232	1344.26 ± 0.768	1510.95 ± 0.565
Exp	1385	1672	1315	1530
	$\boldsymbol{\Lambda_c}$	$\boldsymbol{\Sigma_c}$	$\boldsymbol{\Sigma_c^*}$	$\boldsymbol{\Xi_c}$
ChQM	2224.08 ± 0.617	2416.80 ± 0.342	2449.04 ± 0.342	2453.80 ± 0.534
Exp	2286	2455	2520	2470
	Ξ_c'	Ξ_c^*	Ξ_{cc}	Ω_c
ChQM	2548.35 ± 0.399	2573.26 ± 0.398	3492.87 ± 0.704	2695.61 ± 0.232
Exp	2578	2645	3519	2695
	Ω_c^*			
ChQM	2713.10 ± 0.232			
Exp	2700			

$$\phi_{B_i} = \left(\frac{2}{3\pi b^2}\right)^{3/4}\left(\frac{2}{4\pi b^2}\right)^{3/4}\exp\left(-\frac{\boldsymbol{\lambda_i}^2}{3b^2} - \frac{\boldsymbol{\rho_i}^2}{4b^2}\right)\eta_{I_iS_i}(B_i)\chi_{c_i}(B_i) \tag{11}$$

Now, we can determine the relative motion wave function by solving the Schrödinger equation. From the variational principle,

$$\langle\delta\Psi''|H - E|\Psi'\rangle = 0 \tag{12}$$

the Hamiltonian in the expression above is Formula (1). After performing the variation, we can obtain the RGM equation:

$$\int H(\boldsymbol{R''}, \boldsymbol{R'})\chi(\boldsymbol{R'})\,d\boldsymbol{R'} = E\int N(\boldsymbol{R''}, \boldsymbol{R'})\chi(\boldsymbol{R'})\,d\boldsymbol{R'} \tag{13}$$

where $H(\boldsymbol{R''},\boldsymbol{R'})$ and $N(\boldsymbol{R''},\boldsymbol{R'})$ are Hamiltonian and norm kernels, specifically expressed as

$$\begin{aligned} H(\boldsymbol{R''},\boldsymbol{R'}) &= \langle \mathcal{A}[\phi_1\phi_2\delta(\boldsymbol{R}-\boldsymbol{R''})]|H|\mathcal{A}[\phi_1\phi_2\delta(\boldsymbol{R}-\boldsymbol{R'})]\rangle \\ N(\boldsymbol{R''},\boldsymbol{R'}) &= \langle \mathcal{A}[\phi_1\phi_2\delta(\boldsymbol{R}-\boldsymbol{R''})]|\mathcal{A}[\phi_1\phi_2\delta(\boldsymbol{R}-\boldsymbol{R'})]\rangle \end{aligned} \tag{14}$$

Since the operator $\mathcal{A}$ is Hermitian, satisfying $\mathcal{A}H = H\mathcal{A}$, $\mathcal{A}^2 = \mathcal{A}$, the above expression can be written as

$$\begin{aligned} H(\boldsymbol{R''},\boldsymbol{R'}) &= \langle [\phi_1\phi_2\delta(\boldsymbol{R}-\boldsymbol{R''})]|H|\mathcal{A}[\phi_1\phi_2\delta(\boldsymbol{R}-\boldsymbol{R'})]\rangle \\ N(\boldsymbol{R''},\boldsymbol{R'}) &= \langle [\phi_1\phi_2\delta(\boldsymbol{R}-\boldsymbol{R''})]|\mathcal{A}[\phi_1\phi_2\delta(\boldsymbol{R}-\boldsymbol{R'})]\rangle \end{aligned} \tag{15}$$

the operator $\mathcal{A}$ can be written as $\mathcal{A} = 1 + \mathcal{A}'$, in which $\mathcal{A}'$ represents antisymmetrization operator acting between the two quark clusters. Thus, $H(\boldsymbol{R''},\boldsymbol{R'})$ and $N(\boldsymbol{R''},\boldsymbol{R'})$ can be expressed as the sum of direct terms and exchange terms:

$$\begin{aligned} H(\boldsymbol{R''},\boldsymbol{R'}) &= H^D(\boldsymbol{R''},\boldsymbol{R'})\delta(\boldsymbol{R}-\boldsymbol{R''}) + H^{EX}(\boldsymbol{R''},\boldsymbol{R'}) \\ N(\boldsymbol{R''},\boldsymbol{R'}) &= N^D(\boldsymbol{R''},\boldsymbol{R'})\delta(\boldsymbol{R}-\boldsymbol{R''}) + N^{EX}(\boldsymbol{R''},\boldsymbol{R'}) \end{aligned} \tag{16}$$

where the superscript D represents the direct item, and the superscript EX represents the exchange item. Then, integrate with respect to the coordinates $\boldsymbol{\rho_1}$, $\boldsymbol{\rho_2}$, $\boldsymbol{\lambda_1}$, $\boldsymbol{\lambda_2}$, and $\boldsymbol{R}$ and we can obtain the formula

$$\begin{aligned} \begin{pmatrix} N^D(\boldsymbol{R''},\boldsymbol{R'}) \\ H^D(\boldsymbol{R''},\boldsymbol{R'}) \end{pmatrix}\delta(\boldsymbol{R''}-\boldsymbol{R'}) = \int \phi_1^*(\boldsymbol{\rho_1},\boldsymbol{\lambda_1})\phi_2^*(\boldsymbol{\rho_2},\boldsymbol{\lambda_2})\delta(\boldsymbol{R}-\boldsymbol{R''})\begin{pmatrix} 1 \\ H \end{pmatrix} \\ \times \phi_1(\boldsymbol{\rho_1},\boldsymbol{\lambda_1})\phi_2(\boldsymbol{\rho_2},\boldsymbol{\lambda_2})\delta(\boldsymbol{R}-\boldsymbol{R'})\,d\boldsymbol{\rho_1}\,d\boldsymbol{\lambda_1}\,d\boldsymbol{\rho_2}\,d\boldsymbol{\lambda_2}\,d\boldsymbol{R} \end{aligned} \tag{17}$$

$$\begin{aligned} \begin{pmatrix} N^{EX}(\boldsymbol{R''},\boldsymbol{R'}) \\ H^{EX}(\boldsymbol{R''},\boldsymbol{R'}) \end{pmatrix} = \int \phi_1^*(\boldsymbol{\rho_1},\boldsymbol{\lambda_1})\phi_2^*(\boldsymbol{\rho_2},\boldsymbol{\lambda_2})\delta(\boldsymbol{R}-\boldsymbol{R''})\begin{pmatrix} 1\mathcal{A}'' \\ H\mathcal{A}'' \end{pmatrix} \\ \times \phi_1(\boldsymbol{\rho_1},\boldsymbol{\lambda_1})\phi_2(\boldsymbol{\rho_2},\boldsymbol{\lambda_2})\delta(\boldsymbol{R}-\boldsymbol{R'})\,d\boldsymbol{\rho_1}\,d\boldsymbol{\lambda_1}\,d\boldsymbol{\rho_2}\,d\boldsymbol{\lambda_2}\,d\boldsymbol{R} \end{aligned} \tag{18}$$

So, Formula (13) can be written as

$$\int L(\boldsymbol{R''},\boldsymbol{R'})\chi(\boldsymbol{R'})\,d\boldsymbol{R'} = 0 \tag{19}$$

where

$$\begin{aligned} L(\boldsymbol{R''},\boldsymbol{R'}) =& H(\boldsymbol{R''},\boldsymbol{R'}) - EN(\boldsymbol{R''},\boldsymbol{R'}) \\ =& \left[-\frac{\nabla^2_{\boldsymbol{R'}}}{2\mu} + V^D_{rel}(\boldsymbol{R'}) - E_{rel}\right]\delta(\boldsymbol{R''}-\boldsymbol{R'}) \\ &+ H^{EX}(\boldsymbol{R''},\boldsymbol{R'}) - EN^{EX}(\boldsymbol{R''},\boldsymbol{R'}) \end{aligned} \tag{20}$$

In the above equation, the approximate mass for the two-quark system is defined as μ. $E_{rel} = E - E_{int}$ denotes the relative motion energy, and V^D_{rel} represents the direct term in the interaction potential.

Formula (19) is a differential–integral equation that is difficult to solve. Therefore, we will not directly solve this equation here but will expand the relative motion wave

function $\chi(\boldsymbol{R})$ using a series of known Gaussian wave functions with different generating coordinates $\boldsymbol{S}_i$ ($i = 1,\ 2,\ \cdots n$):

$$\chi(\boldsymbol{R}) = \frac{1}{\sqrt{4\pi}}\left(\frac{3}{2\pi b^2}\right)^{3/4}\sum_{i=1}^{n} C_i \times \int \exp\left[-\frac{3}{4b^2}(\boldsymbol{R}-\boldsymbol{S}_i)^2\right] Y_{LM}(\hat{\boldsymbol{S}}_i)\, d\hat{\boldsymbol{S}}_i \tag{21}$$

where L denotes the orbital angular momentum between the two clusters. As all systems studied in this work are S-waves, $L = 0$. The center of mass motion wave function is

$$Z(\boldsymbol{R}_c) = \left(\frac{6}{\pi b^2}\right)^{3/4} e^{-\frac{3\boldsymbol{R}_c^2}{b^2}} \tag{22}$$

and, for the orbital wave functions, $\phi_\alpha(\boldsymbol{S}_i)$ and $\phi_\beta(-\boldsymbol{S}_i)$ represent single-particle orbital wave functions centered at different reference points:

$$\begin{aligned}\phi_\alpha(\boldsymbol{S}_i) &= \left(\frac{1}{\pi b^2}\right)^{\frac{3}{4}} e^{-\frac{(r_\alpha - \boldsymbol{S}_i/2)^2}{2b^2}},\\ \phi_\beta(-\boldsymbol{S}_i) &= \left(\frac{1}{\pi b^2}\right)^{\frac{3}{4}} e^{-\frac{(r_\beta + \boldsymbol{S}_i/2)^2}{2b^2}}\end{aligned} \tag{23}$$

Formula (10) can be rewritten by substituting Formulas (21)–(23):

$$\Psi_{6q} = \sum_{i=1}^{n} C_i \psi_i \tag{24}$$

$$= \mathcal{A}\sum_{i=1}^{n} C_i \int \frac{d\hat{\boldsymbol{S}}_i}{\sqrt{4\pi}} \prod_{\alpha=1}^{3}\phi_\alpha(\boldsymbol{S}_i)\prod_{\beta=4}^{6}\phi_\beta(-\boldsymbol{S}_i) \times \left[\left[\eta_{I_1S_1}(B_1)\eta_{I_2S_2}(B_2)\right]^{IS} Y_{LM}(\hat{\boldsymbol{S}}_i)\right]^{J} \times \left[\chi_c(B_1)\chi_c(B_2)\right]^{[\sigma]}, \tag{25}$$

Finally, substituting Formula (21) into Formula (13) leads to the algebraic form of the RGM equation:

$$\sum_j C_j H_{i,j} = E\sum_j C_j N_{i,j}. \tag{26}$$

where $H_{i,j}$ represents the Hamiltonian matrix elements ($H_{ij} = \langle\psi_i|H|\psi_j\rangle$), and $N_{i,j}$ is the overlap ($N_{ij} = \langle\psi_i|\psi_j\rangle$). By solving Equation (26), the energy and wave function of the six-quark system can be obtained. More details on the resonating group method can be found in Ref. [34].

3. Results and Discussion

In this work, we systematically investigate S-wave singly charmed ($C = 1$) dibaryon states with the angular momentum $J = 1$, isospin $I = 0,\ \frac{1}{2},\ 1,\ \frac{3}{2},\ 2,\ \frac{5}{2}$, and strangeness $S = -1,\ -2,\ -3,\ -4,\ -5$. In the following discussion, we will first introduce the construction of the wave function, study the interaction between two baryons by calculating the effective potentials, and finally perform bound-state calculations on the system to search for possible dibaryon states.

3.1. Wave Function Construction

The total wave function of the six-quark system consists of spatial, flavor, spin, and color components. The detailed construction of the spatial wave function is presented in Section 2.2. Here, we introduce the wave functions of baryons and dibaryons separately. Due to the numerous channels involved in the system, we will use $N\Xi_c$ as an example for detailed elaboration.

In order to construct the wave function of the six-quark system, we must first construct the baryon wave functions. For the $N\Xi_c$ channel, the involved baryons are $p(uud)$, $n(udd)$, $\Xi_c^0(dsc)$, $\Xi_c^+(usc)$. The spin, flavor, and color wave functions of these four baryons will be presented in detail below.

(1) Baryon spin wave functions: The system involves a total of 8 distinct spin wave functions, as detailed in Ref. [30]. The spin wave functions used in this channel are listed below:

$$\chi^{\sigma 1}_{\frac{1}{2},\frac{1}{2}} = \frac{1}{\sqrt{6}}(2\alpha\alpha\beta - \alpha\beta\alpha - \beta\alpha\alpha)$$
$$\chi^{\sigma 2}_{\frac{1}{2},\frac{1}{2}} = \frac{1}{\sqrt{2}}(\alpha\beta\alpha - \beta\alpha\alpha)$$

where the symbol α represents the spin-up state; the symbol β represents the spin-down state. We use χ^{σ}_{S,S_z} to denote the baryon spin wave function, where S and S_z represent the spin quantum number and its third component, respectively. For wave functions with identical quantum numbers but different symmetries, we distinguish them using different superscripts. For example: $\chi^{\sigma 1}_{\frac{1}{2},\frac{1}{2}}$ and $\chi^{\sigma 2}_{\frac{1}{2},\frac{1}{2}}$ represent symmetric and antisymmetric wave functions with spin quantum number $\frac{1}{2}$.

(2) Baryon flavor wave functions: The system involves a total of 36 distinct flavor wave function configurations, as detailed in Ref. [30]. The flavor wave functions for these four baryons are, respectively, expressed as

$$\chi^{f1}_{\frac{1}{2},\frac{1}{2}} = \sqrt{\frac{1}{6}}(2uud - udu - duu)$$
$$\chi^{f2}_{\frac{1}{2},\frac{1}{2}} = \sqrt{\frac{1}{2}}(udu - duu)$$
$$\chi^{f3}_{\frac{1}{2},-\frac{1}{2}} = \sqrt{\frac{1}{6}}(udd + dud - 2ddu)$$
$$\chi^{f4}_{\frac{1}{2},-\frac{1}{2}} = \sqrt{\frac{1}{2}}(udd - dud)$$
$$\chi^{f1}_{\frac{1}{2},-\frac{1}{2}} = \frac{1}{2}(dcs + cds - csd - scd)$$
$$\chi^{f2}_{\frac{1}{2},-\frac{1}{2}} = \sqrt{\frac{1}{12}}(2dsc - 2sdc + csd + dcs - cds - scd)$$
$$\chi^{f3}_{\frac{1}{2},\frac{1}{2}} = \frac{1}{2}(ucs + cus - csu - scu)$$
$$\chi^{f4}_{\frac{1}{2},\frac{1}{2}} = \sqrt{\frac{1}{12}}(2usc - 2suc + csu + ucs - cus - scu)$$

Similar to the spin wave function, we use χ^{f}_{I,I_z} to denote the baryon flavor wave function, where I and I_z represent the isospin quantum number and its third component, respectively. Here, both light quarks and heavy quarks are treated as identical particles with $SU(4)$ symmetry.

(3) Baryon color wave function: Each quark carries one of three color charges: red (r), green (g), or blue (b). As is well known, all physically observed hadronic states must

be color singlets (colorless), which implies that the color wave function must be fully antisymmetric. The color wave function for a baryon cluster can be expressed as

$$\chi^c = \sqrt{\frac{1}{6}}(rgb - rbg + gbr - grb + brg - bgr)$$

Since the spin, flavor, and color degrees of freedom are independent, we directly multiply the three parts of the wave functions to obtain the total wave function of the baryon, denoted as $\phi^B_{I_z,S_z}$, where I_z is the third component of isospin, S_z represents the third component of spin, and B denotes the baryon. The system involves a total of 80 distinct baryon wave functions, as detailed in Ref. [30]. The wave functions of the four baryons can be expressed as

$$\begin{aligned}
\phi^{p}_{\frac{1}{2},\frac{1}{2}} &= \sqrt{\frac{1}{2}}\left(\chi^{f1}_{\frac{1}{2},\frac{1}{2}}\chi^{\sigma 1}_{\frac{1}{2},\frac{1}{2}} + \chi^{f2}_{\frac{1}{2},\frac{1}{2}}\chi^{\sigma 2}_{\frac{1}{2},\frac{1}{2}}\right)\chi^c \\
\phi^{\Xi_c}_{-\frac{1}{2},\frac{1}{2}} &= \sqrt{\frac{1}{2}}\left(\chi^{f1}_{\frac{1}{2},-\frac{1}{2}}\chi^{\sigma 1}_{\frac{1}{2},\frac{1}{2}} + \chi^{f2}_{\frac{1}{2},-\frac{1}{2}}\chi^{\sigma 2}_{\frac{1}{2},\frac{1}{2}}\right)\chi^c \\
\phi^{n}_{-\frac{1}{2},\frac{1}{2}} &= \sqrt{\frac{1}{2}}\left(\chi^{f3}_{\frac{1}{2},-\frac{1}{2}}\chi^{\sigma 1}_{\frac{1}{2},\frac{1}{2}} + \chi^{f4}_{\frac{1}{2},-\frac{1}{2}}\chi^{\sigma 2}_{\frac{1}{2},\frac{1}{2}}\right)\chi^c \\
\phi^{\Xi_c}_{\frac{1}{2},\frac{1}{2}} &= \sqrt{\frac{1}{2}}\left(\chi^{f3}_{\frac{1}{2},\frac{1}{2}}\chi^{\sigma 1}_{\frac{1}{2},\frac{1}{2}} + \chi^{f4}_{\frac{1}{2},\frac{1}{2}}\chi^{\sigma 2}_{\frac{1}{2},\frac{1}{2}}\right)\chi^c
\end{aligned}$$

By substituting the wave functions of the flavor, spin, and color components according to the given quantum numbers of the system, the total flavor–spin–color wave function of the dibaryon system can be obtained. The wave function of the dibaryon is then constructed by coupling the two baryon wave functions using Clebsch–Gordan coefficients according to the total quantum numbers. Therefore, the wave function of $N\Xi_c$ is expressed as

$$|N\Xi_c\rangle = \sqrt{\frac{1}{2}}\left[\phi^{p}_{\frac{1}{2},\frac{1}{2}}\phi^{\Xi_c}_{-\frac{1}{2},\frac{1}{2}} - \phi^{n}_{-\frac{1}{2},\frac{1}{2}}\phi^{\Xi_c}_{\frac{1}{2},\frac{1}{2}}\right]$$

All possible channels are listed in Table 3.

Table 3. The channels involved in the calculation.

I	S	*Channels*
0	-1	$\Lambda\Lambda_c$ $N\Xi_c$ $N\Xi_c'$ $N\Xi_c^*$ $\Sigma\Sigma_c$ $\Sigma\Sigma_c^*$ $\Sigma^*\Sigma_c$ $\Sigma^*\Sigma_c^*$
	-3	$\Lambda\Omega_c$ $\Lambda\Omega_c^*$ $\Lambda_c\Omega$ $\Xi\Xi_c$ $\Xi\Xi_c^{'}$ $\Xi\Xi_c^*$ $\Xi^*\Xi_c$ $\Xi^*\Xi_c^*$ $\Xi^*\Xi_c^{'}$
	-5	$\Omega\Omega_c$ $\Omega\Omega_c^*$
$\frac{1}{2}$	0	$N\Sigma_c$ $N\Sigma_c^*$ $\Sigma_c\Delta$ $\Sigma_c^*\Delta$
	-2	$\Sigma_c\Xi$ $\Sigma\Xi_c$ $\Sigma\Xi_c'$ $\Sigma_c\Xi^*$ $\Sigma\Xi_c^*$ $\Xi\Sigma_c^*$ $\Xi_c\Sigma^*$ $\Xi_c'\Sigma^*$ $\Xi^*\Sigma_c^*$ $\Xi_c^*\Sigma^*$
1	-1	$\Sigma\Sigma_c$ $N\Xi_c$ $N\Xi_c'$ $\Lambda\Sigma_c$ $\Lambda_c\Sigma$ $\Lambda\Sigma_c^*$ $\Lambda_c\Sigma^*$
		$N\Xi_c^*$ $\Xi_c\Delta$ $\Xi_c'\Delta$ $\Sigma\Sigma_c^*$ $\Sigma_c\Sigma^*$ $\Xi_c^*\Delta$ $\Sigma^*\Sigma_c^*$
	-3	$\Sigma\Omega_c$ $\Xi\Xi_c$ $\Sigma_c\Omega$ $\Sigma\Omega_c^*$ $\Xi_c'\Xi^*$
		$\Xi_c\Xi^*$ $\Xi\Xi_c^*$ $\Sigma^*\Omega_c$ $\Omega\Sigma_c^*$ $\Sigma^*\Omega_c^*$ $\Xi^*\Xi_c^*$
$\frac{3}{2}$	0	$\Sigma_c N$ $\Sigma_c^* N$ $\Sigma_c\Delta$ $\Sigma_c^*\Delta$
	-2	$\Sigma_c\Xi$ $\Sigma\Xi_c$ $\Sigma\Xi_c'$ $\Sigma_c\Xi^*$ $\Sigma\Xi_c^*$ $\Xi\Sigma_c^*$ $\Xi_c\Sigma^*$ $\Xi_c'\Sigma^*$ $\Xi^*\Sigma_c^*$ $\Xi_c^*\Sigma^*$
2	-1	$\Xi_c\Delta$ $\Xi_c'\Delta$ $\Sigma\Sigma_c^*$ $\Sigma_c\Sigma^*$ $\Sigma\Sigma_c$ $\Xi_c^*\Delta$ $\Sigma^*\Sigma_c^*$
$\frac{5}{2}$	0	$\Sigma_c\Delta$ $\Sigma_c^*\Delta$

3.2. The Effective Potential

In particle physics, the effective potential refers to a simplified model potential that describes interparticle interactions by integrating out microscopic degrees of freedom and reducing complex many-body interactions to an equivalent particle- or two-body potential

function [35]. In this work, the effective potential between the two baryons can be expressed in the following form:

$$V(S_i) = E(S_i) - E(\infty) \tag{27}$$

The symbol S_i denotes the distance between the two baryon clusters, $E(\infty)$ represents the interaction energy at a sufficiently large separation distance, and $E(S_i)$ is explicitly given by

$$E(S_i) = \frac{\langle \Psi_{6q}(S_i) \,|\, H \,|\, \Psi_{6q}(S_i) \rangle}{\langle \Psi_{6q}(S_i) | \Psi_{6q}(S_i) \rangle} \tag{28}$$

$\Psi_{6q}(S_i)$ represents the specific wave function of a dibaryon state; $\langle \Psi_{6q}(S_i) \,|\, H \,|\, \Psi_{6q}(S_i) \rangle$ and $\langle \Psi_{6q}(S_i) | \Psi_{6q}(S_i) \rangle$ are Hamiltonian matrix and the overlap of the states. The overlap of the states is always positive, so the sign variation of the effective potential cannot be caused by the scalar product between wave functions. The effective potentials for systems with different quantum numbers and varying strange quarks are presented in Figures 1–11. Although most of them have attractive and repulsive regions, as long as there is a negative minimum potential between two hadrons, it indicates the existence of an attractive potential between these two hadrons, which may form a bound state.

For the $I = 0,\ S = -1$ system, the effective potentials of different channels are shown in Figure 1. Among these eight channels, only the $N\Xi_c^*$ channel exhibits a purely repulsive interaction, while the other seven channels all exhibit attractive potentials. Additionally, the effective potential of $\Sigma\Sigma_c$, $\Sigma\Sigma_c^*$, $\Sigma^*\Sigma_c$, and $\Sigma^*\Sigma_c^*$ is deeper than that of the other three channels, indicating that these four channels are more prone to forming bound states. The attractive potential region of $\Sigma\Sigma_c$ is 0.5–2 fm, and the deepest attractive potential has a value of about 100 MeV at a distance of around 1 fm between the two clusters. Meanwhile, the repulsive potential region of $\Sigma\Sigma_c$ is 0–0.5 fm.

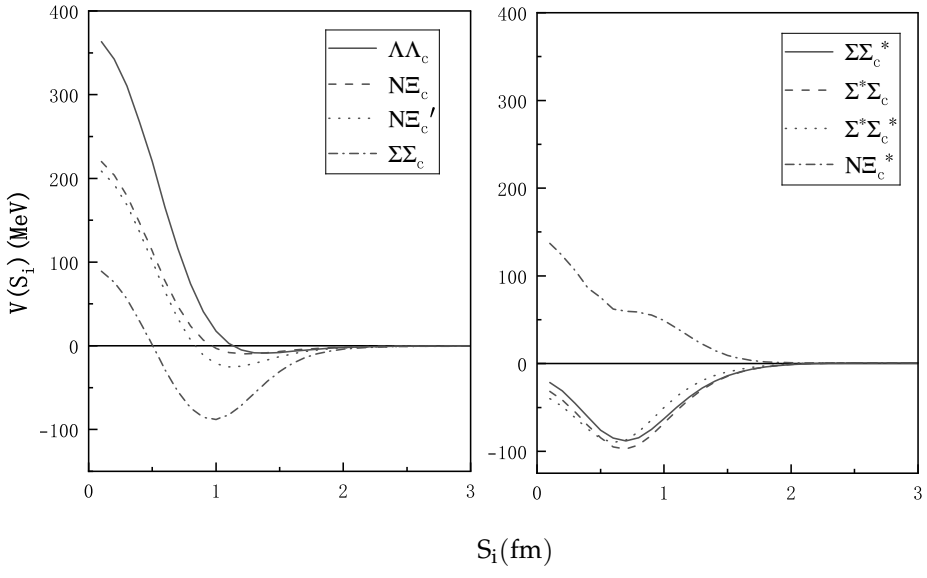

Figure 1. The effective potentials of different channels of the singly charmed dibaryons with $I = 0,\ S = -1$. All states exhibit attractive potentials except $N\Xi_c^*$ (double-dot dash).

For the $I = 0,\ S = -3$ system, the effective potentials of different channels are shown in Figure 2. $\Lambda\Omega_c^*$, $\Xi\Xi_c$, $\Xi\Xi_c^*$, $\Xi^*\Xi_c'$ and $\Xi^*\Xi_c^*$ channels exhibit attractive potentials, while the other four channels have purely repulsive potentials. Also, the effective potentials of $\Xi\Xi_c$ and $\Xi\Xi_c^*$ are deeper than that of the other three channels, indicating that these two channels are more prone to forming bound states. Meanwhile, the attractive potential

region of $\Xi\Xi_c$ is 0.6–2 fm, and the repulsive potential region of this state is 0–0.6 fm. The deepest attractive potential is less than 50 MeV at a distance of around 1 fm between the two clusters.

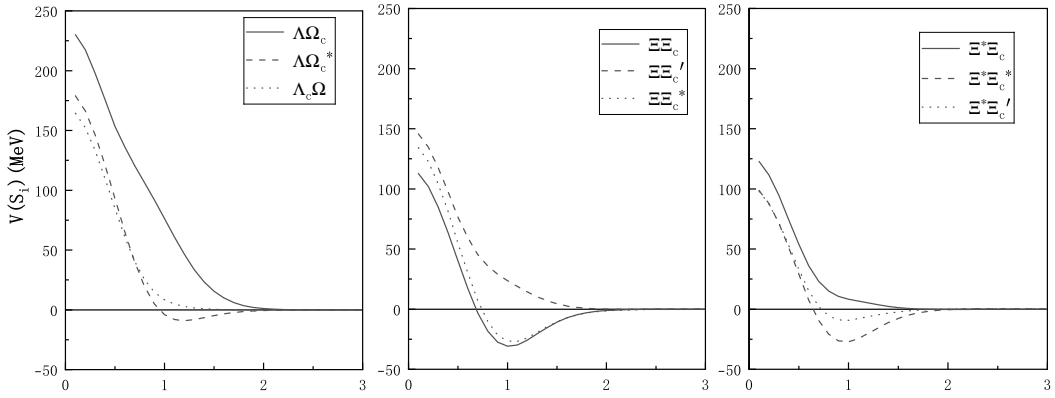

Figure 2. The effective potentials of different channels of the singly charmed dibaryons with $I = 0,\ S = -3$. All states exhibit attractive potentials except $\Lambda\Omega_c$, $\Lambda_c\Omega$, $\Xi\Xi_c'$, $\Xi^*\Xi_c$.

For the $I = 0,\ S = -5$ system, the effective potentials of different channels are shown in Figure 3. We can identify two distinct channels in this system. Both $\Omega\Omega_c$ and $\Omega\Omega_c^*$ states exhibit a weakly attractive potential. Consequently, we conclude that neither channel is likely to form bound states.

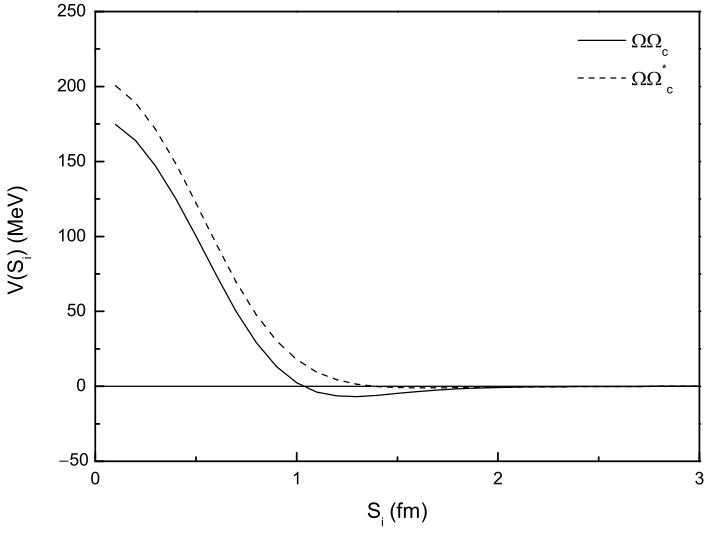

Figure 3. The effective potentials of different channels of the singly charmed dibaryons with $I = 0,\ S = -5$. Both $\Omega\Omega_c$ and $\Omega\Omega_c^*$ states exhibit attractive potentials.

For $I = \frac{1}{2},\ S = 0$ system, the effective potentials of different channels are shown in Figure 4. It can be observed that this system exhibits four distinct channels, among which only the $N\Sigma_c^*$ channel has purely repulsive interactions, while the other three channels exhibit attractive interactions. Furthermore, the effective potentials of both the $\Sigma_c\Delta$ and $\Sigma_c^*\Delta$ are deeper than the $N\Sigma_c$ state. In comparison, the $\Sigma_c\Delta$ and $\Sigma_c^*\Delta$ are more likely to form bound states. Meanwhile, the attractive potential region of $\Sigma_c^*\Delta$ is 0–2 fm, and the deepest attractive potential is more than 100 MeV at a distance of around 0.6 fm between the two clusters.

For the $I = \frac{1}{2},\ S = -2$ system, the effective potentials of different channels are shown in Figure 5. Among these ten channels, only the $\Sigma\Xi_c^*$ channel has a purely repulsive effective potential, while the other nine channels all exhibit attractive interactions. Furthermore,

within these nine attractive channels, we note that four specific channels, $\Sigma_c\Xi$, $\Sigma\Xi_c$, $\Xi\Sigma_c^*$, and $\Xi_c'\Sigma^*$, exhibit significantly deeper effective potentials, indicating their greater propensity to form bound states. Meanwhile, the attractive potential region of $\Sigma_c\Xi$, $\Sigma\Xi_c$, $\Xi\Sigma_c^*$, and $\Xi_c'\Sigma^*$ is 0.6–2 fm, and the deepest attractive potential is more than 25 MeV at a distance of around 1 fm between the two clusters. The repulsive potential region of these states is 0–0.6 fm.

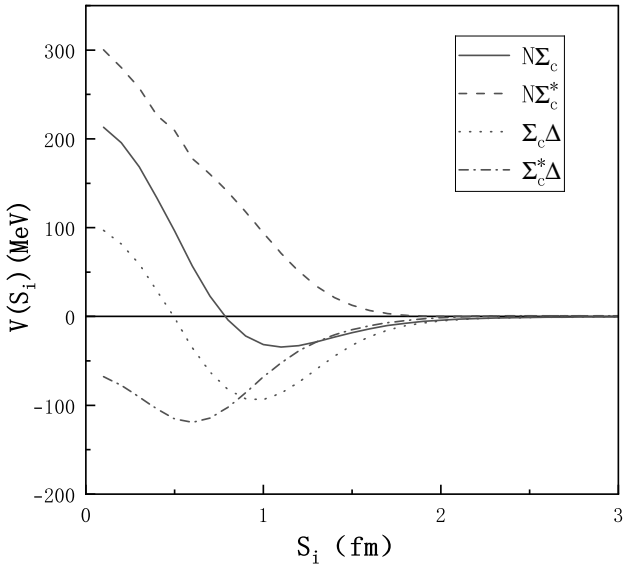

Figure 4. The effective potentials of different channels of the singly charmed dibaryons with $I = \frac{1}{2}$, $S = 0$. All states exhibit attractive potentials except $N\Sigma_c^*$ (dashed line).

For the $I = 1$, $S = -1$ system, the effective potentials of different channels are shown in Figure 6. Among these fourteen channels, a total of seven channels exhibit attractive interactions, specifically $\Sigma\Sigma_c$, $\Xi_c\Delta$, $\Xi_c'\Delta$, $\Sigma\Sigma_c^*$, $\Sigma_c\Sigma^*$, $\Xi_c^*\Delta$, $\Sigma^*\Sigma_c^*$, while all other channels have purely repulsive behavior. Furthermore, the effective potential of the $\Sigma\Sigma_c$ state is deeper than the seven other channels. We therefore conclude that the $\Sigma\Sigma_c$ state is more likely to form bound states. Meanwhile, the attractive potential region of $\Sigma\Sigma_c$ is 0.5–2 fm, and the deepest attractive potential is close to 25 MeV at a distance of around 0.9 fm between the two clusters. The repulsive potential region of this state is 0–0.5 fm.

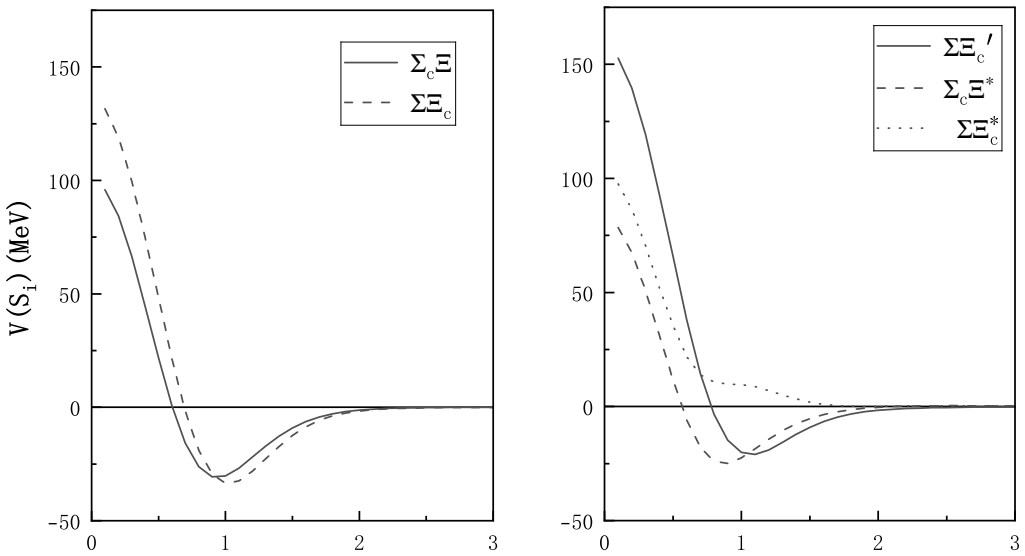

Figure 5. *Cont.*

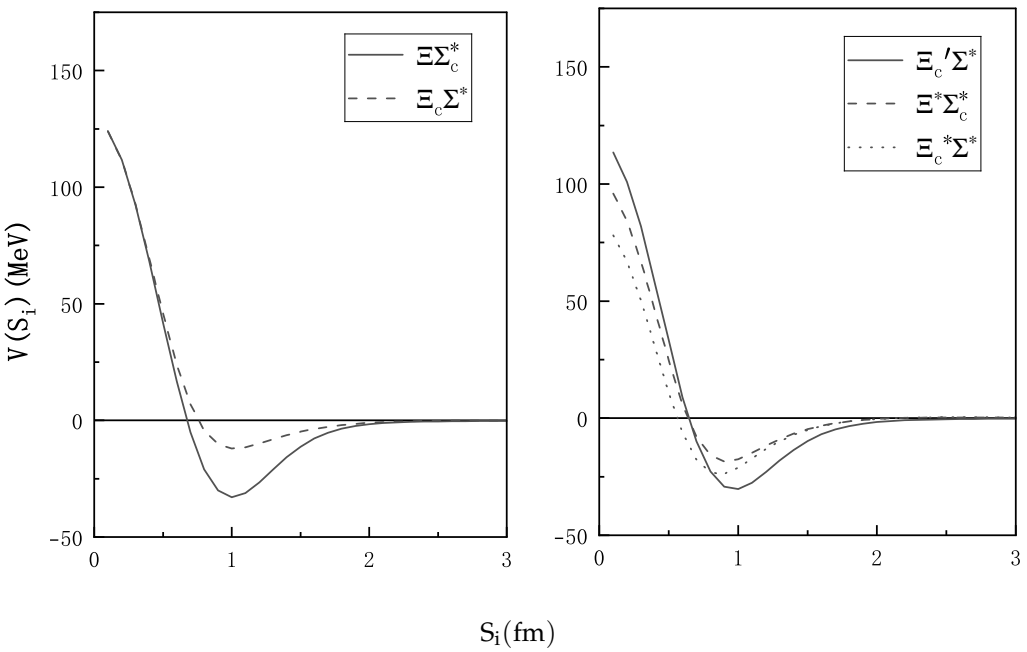

Figure 5. The ffective potentials of different channels of the singly charmed dibaryons with $I = \frac{1}{2}$, $S = -2$. All states exhibit attractive potentials except $\Sigma\Xi_c^*$ (dotted line).

For the $I = 1$, $S = -3$ system, the effective potentials of different channels are shown in Figure 7. Only the $\Xi_c'\Xi^*$ state exhibits a very weakly attractive effective potential, while all other channels have purely repulsive interactions. Consequently, bound-state formation is unlikely in this system.

For the $I = \frac{3}{2}$, $S = 0$ system, the effective potentials of different channels are shown in Figure 8. The $N\Sigma_c$ channel has a purely repulsive potential. The remaining three channels, $N\Sigma_c^*$, $\Sigma_c\Delta$, and $\Sigma_c^*\Delta$, exhibit attractive potentials, with the $\Sigma_c\Delta$ channel showing deeper potential compared to the other two, indicating a greater propensity for bound-state formation. Meanwhile, the attractive potential region of $\Sigma_c\Delta$ is 0.6–2 fm, and the deepest attractive potential is more than 25 MeV at a distance of around 1 fm between the two clusters. The repulsive potential region of this state is 0–0.6 fm.

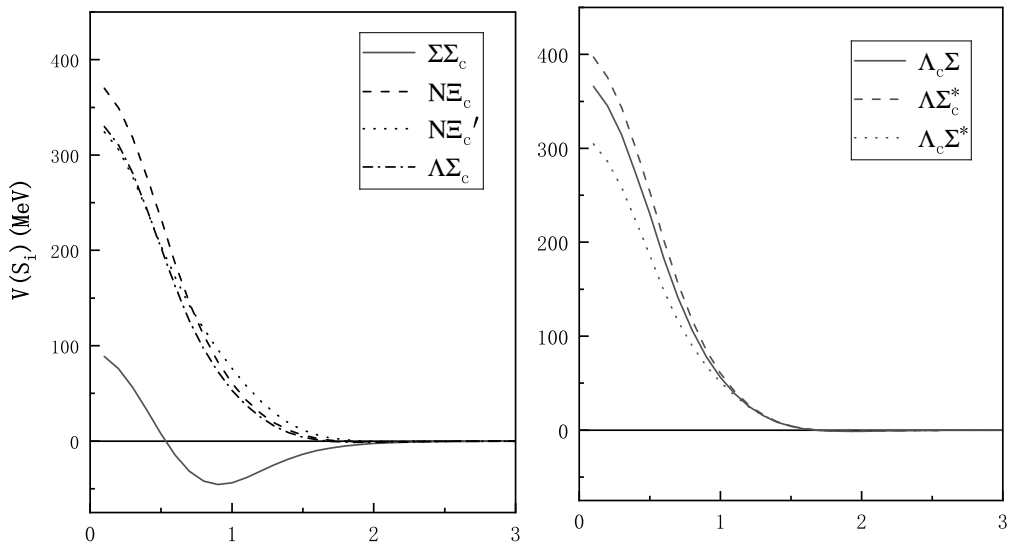

Figure 6. *Cont.*

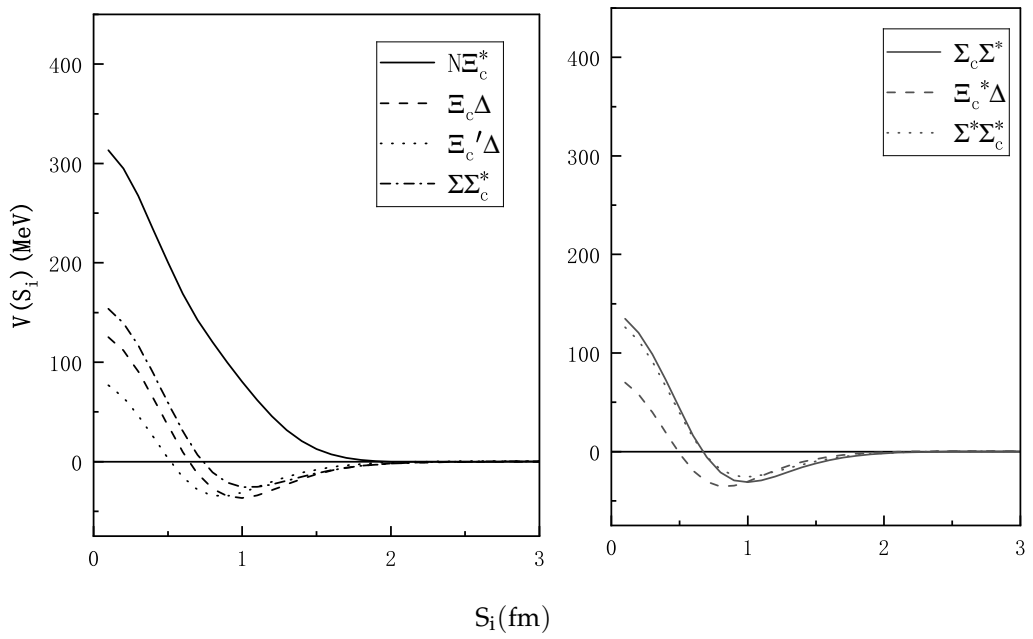

Figure 6. The effective potentials of different channels of the singly charmed dibaryons with $I = 1$, $S = -1$. The $\Sigma\Sigma_c$, $\Xi_c\Delta$, $\Xi_c'\Delta$, $\Sigma\Sigma_c^*$, $\Sigma_c\Sigma^*$, $\Xi_c^*\Delta$, $\Sigma^*\Sigma_c^*$ channels exhibit attractive potentials and the other channels have a purely repulsive potential.

For the $I = \frac{3}{2}$, $S = -2$ system, the effective potentials of different channels are shown in Figure 9. Five states, $\Sigma\Xi_c$, $\Sigma_c\Xi^*$, $\Xi_c'\Sigma^*$ $\Xi^*\Sigma_c^*$, and $\Xi_c^*\Sigma^*$, exhibit very weakly attractive potentials, while other states exhibit purely repulsive behavior. Although these five states exhibit attractive potentials, the potentials are too shallow to support bound-state formation under these conditions.

For the $I = 2$, $S = -1$ system, the effective potentials of different channels are shown in Figure 10. This system contains a total of seven channels, among which the $\Xi_c\Delta$ and $\Sigma\Sigma_c$ channels exhibit purely repulsive interactions, while the remaining channels exhibit weakly attractive potentials. Although these channels exhibit attractive effective potentials, the interaction depths are exceptionally shallow. Consequently, we conclude that no bound states can exist in this system under the given conditions.

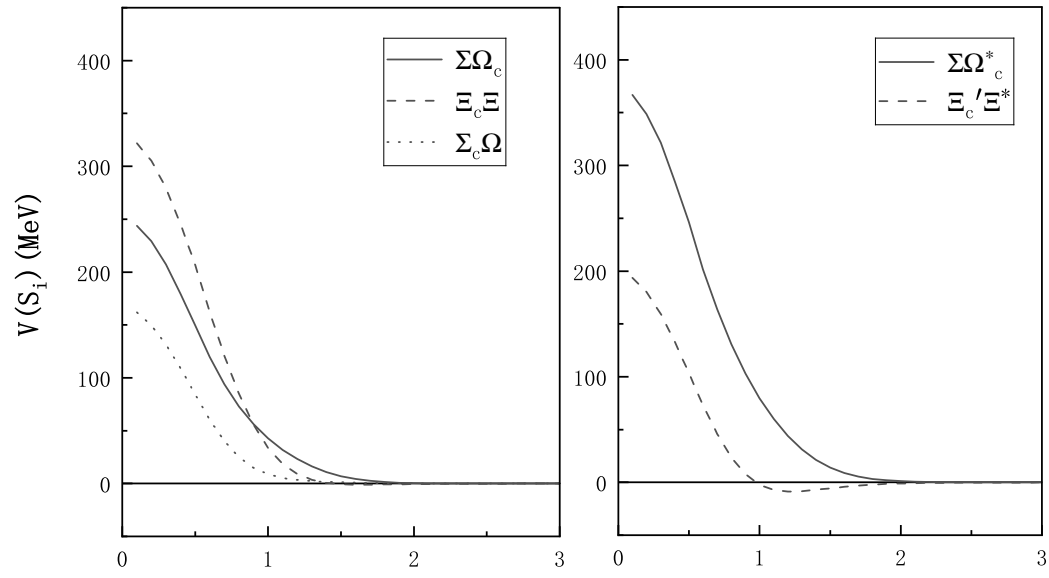

Figure 7. *Cont.*

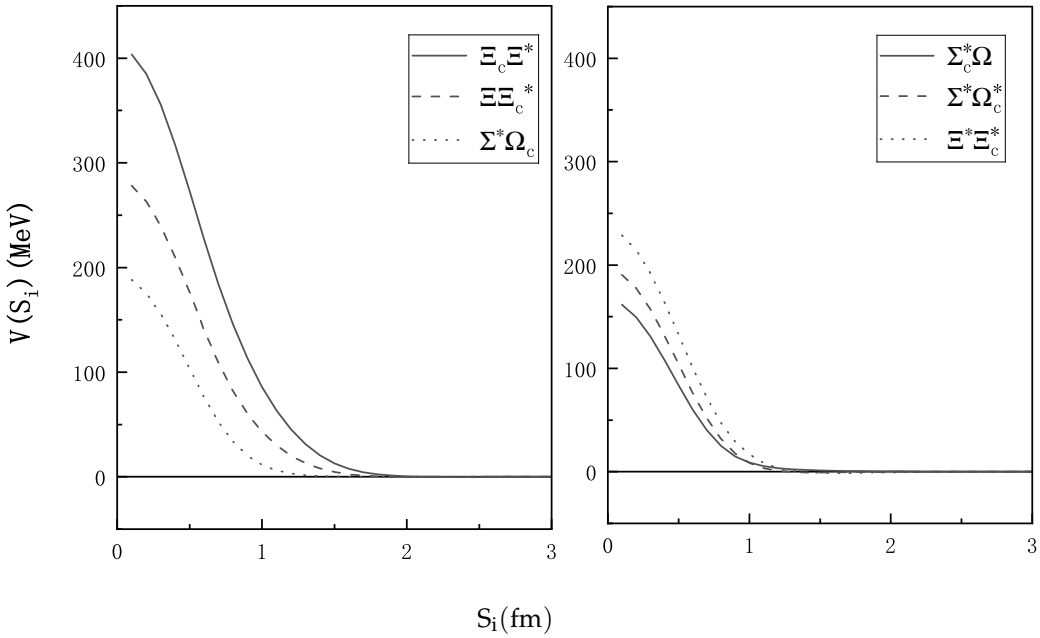

Figure 7. The effective potentials of different channels of the singly charmed dibaryons with $I = 1$, $S = -3$. All states exhibit purely repulsive potentials except $\Xi_c'\Xi^*$ (dashed line).

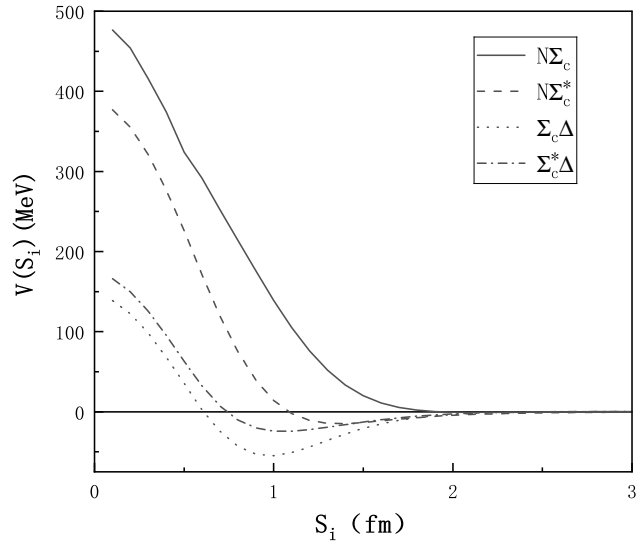

Figure 8. The effective potentials of different channels of the singly charmed dibaryons with $I = \frac{3}{2}$, $S = 0$. All states exhibit attractive potentials except $N\Sigma_c$ (solid line).

For the $I = \frac{5}{2}$, $S = 0$ system, the effective potentials of different channels are shown in Figure 11. We can observe that this system consists of two channels, both exhibiting attractive potentials. The potential well of the $\Sigma_c\Delta$ channel is deeper than that of the $\Sigma_c^*\Delta$ channel. However, the attraction in these two channels is too weak to support a bound state.

From the study of the effective potentials above, it can be observed that some states exhibit deeply attractive interactions, some exhibit weakly attractive interactions, while others are purely repulsive. These findings provide valuable insights for the subsequent research on bound states and resonance states.

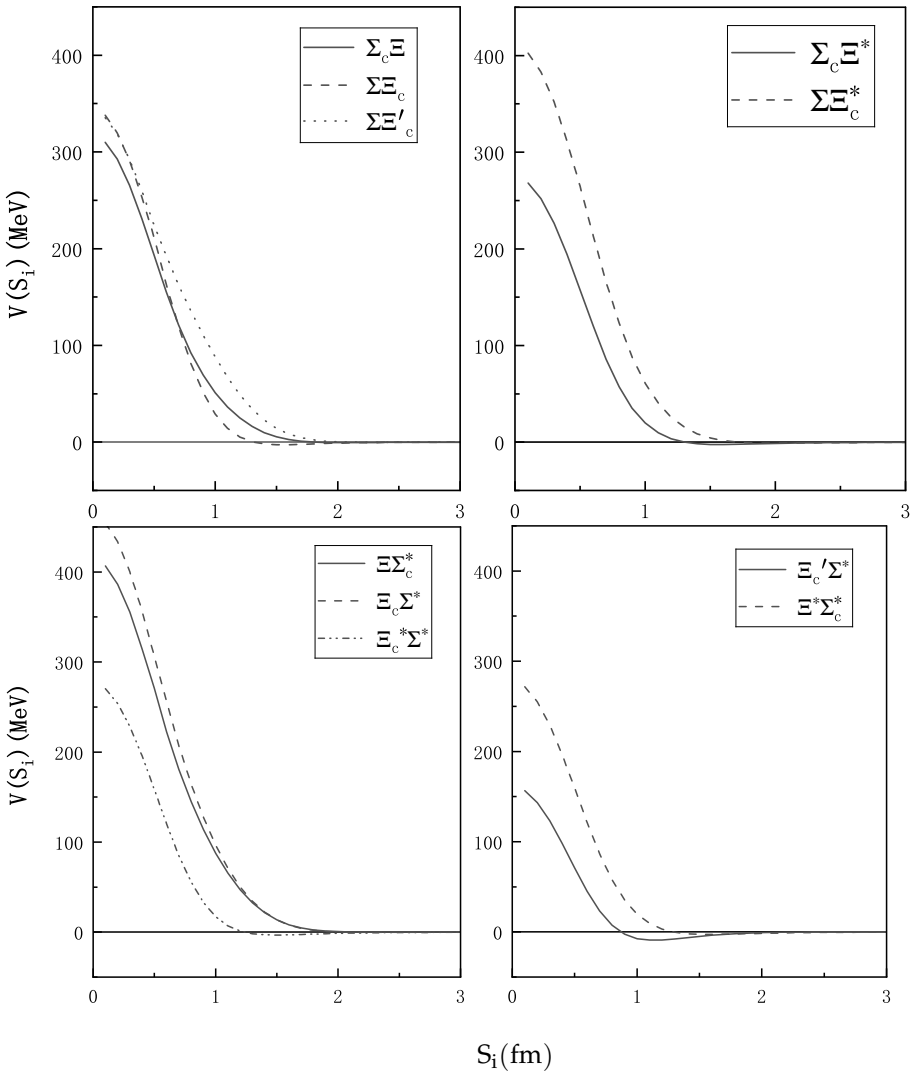

Figure 9. The effective potentials of different channels of the singly charmed dibaryons with $I = \frac{3}{2}$, $S = -2$. All states exhibit attractive potentials except $\Sigma_c\Xi$, $\Sigma\Xi'_c$, $\Sigma\Xi^*_c$, $\Xi\Sigma^*_c$, $\Xi_c\Sigma^*$.

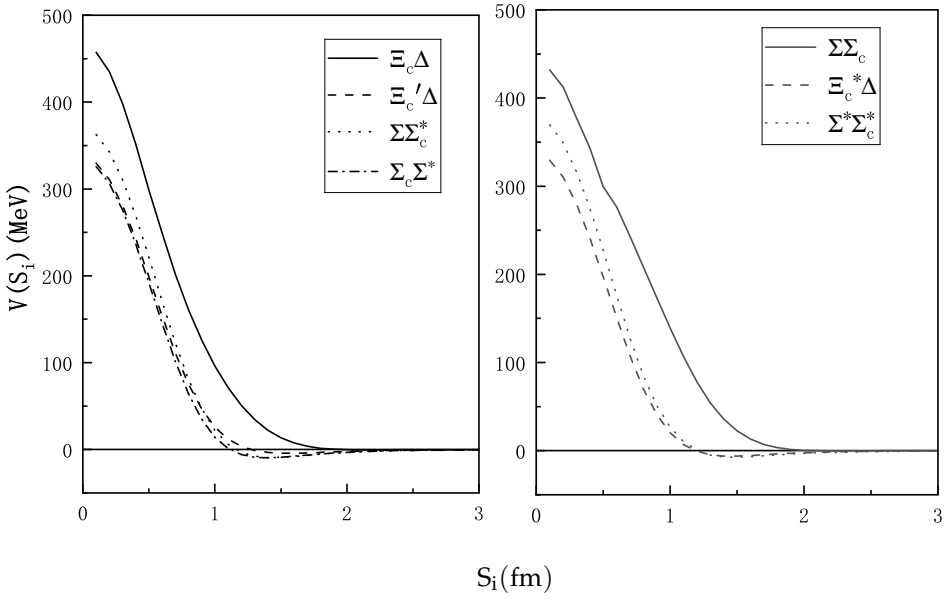

Figure 10. The effective potentials of different channels of the singly charmed dibaryons with $I = 2$, $S = -1$. All states exhibit attractive potentials except $\Xi_c\Delta$ and $\Sigma\Sigma_c$.

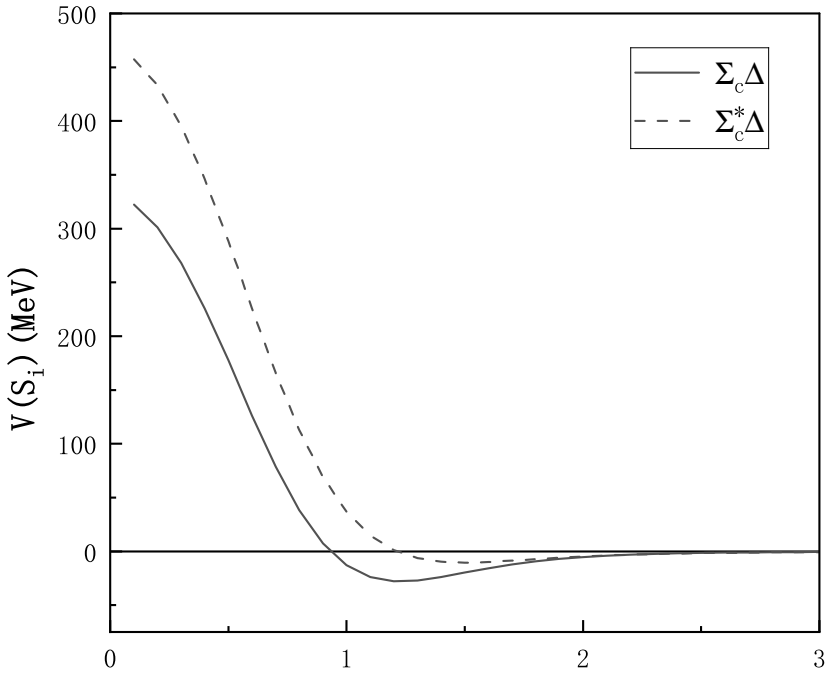

Figure 11. The effective potentials of different channels of the singly charmed dibaryons with $I = \frac{5}{2}$, $S = 0$. All states exhibit attractive potentials.

3.3. Bound-State Calculation

To investigate possible bound states, we conduct systematic bound-state calculations. We calculate the energies of each single channel. Meanwhile, we also consider the effects of channel coupling and perform coupled-channel calculations. The computational results are listed in Tables 4–14. In these tables, the first column indicates the particle species; the second column E_{th} shows the corresponding theoretical thresholds for each state; the third column E_{sc} presents the single-channel energy; the fourth column B_{sc} displays the single-channel binding energy (where $B_{sc} = E_{sc} - E_{th}$). The fifth E_{cc} column provides the lowest energy of the system after channel coupling, and the final column B_{cc} (where $B_{cc} = E_{cc} - E_{th}^{min}$) provides the binding energy from channel coupling. For states where no bound state exists, we denote them with 'ub' (unbound). The calculation results show that the error values of energy in each system caused by parameter errors are very small. Therefore, the results of the these dibaryon systems are not sensitive to parameters.

For the $I = 0$, $S = -1$ system, the energies of different channels are shown in Table 4. Within this system, the single-channel energy calculations demonstrate that four channels, $\Sigma\Sigma_c$, $\Sigma\Sigma_c^*$, $\Sigma^*\Sigma_c$, and $\Sigma^*\Sigma_c^*$, can form bound states with the binding energies of -21.86 ± 1.447 MeV, -24.16 ± 1.471 MeV, -32.19 ± 1.201 MeV, and -25.20 ± 1.208 MeV, respectively. The remaining four channels exhibit energies above the theoretical threshold, which indicates that no bound states are formed in these channels. These results are consistent with the predictions from effective potential analysis. The effective potentials of the four channels ($\Sigma\Sigma_c$, $\Sigma\Sigma_c^*$, $\Sigma^*\Sigma_c$, and $\Sigma^*\Sigma_c^*$) in Figure 1 are relatively deep, approaching 100 MeV, which indicates that the attraction in these four channels is strong enough to form bound states. Although the effective potentials in the three channels ($\Lambda\Lambda_c$, $N\Xi_c$, $N\Xi_c'$) are attractive, the attraction is too weak to form bound states. The remaining channel ($N\Xi_c^*$) exhibits a purely repulsive effective potential, which prevents the bound-state formation. Coupled-channel energy calculations further reveal that the system ground-state energy remains higher than the minimum theoretical threshold $(\Lambda\Lambda_c)$. We therefore conclude that no bound states below the lowest threshold exist in this system. However, there may exist resonance states. For higher-energy single-channel bound states, they may decay to

open channels ($\Lambda\Lambda_c$, $N\Xi_c$, $N\Xi_c'$, and $N\Xi_c^*$), and their existence as resonance states may be verified through scattering processes, which will be investigated in the future.

Table 4. The energy (in MeV) of different channels of the singly charmed dibaryons with $I = 0$, $S = -1$.

Channels	E_{th}	E_{sc}	B_{sc}	E_{cc}	B_{cc}
$\Lambda\Lambda_c$	3328.93 ± 1.635	3337.16 ± 1.163	ub	3335.76 ± 1.176	ub
$N\Xi_c$	3386.50 ± 1.509	3394.06 ± 1.045	ub		
$N\Xi_c'$	3481.05 ± 1.374	3486.15 ± 0.909	ub		
$N\Xi_c^*$	3505.96 ± 1.373	3515.29 ± 0.909	ub		
$\Sigma\Sigma_c$	3624.74 ± 1.220	3602.88 ± 0.779	−21.86 ± 1.447		
$\Sigma\Sigma_c^*$	3656.98 ± 1.220	3632.82 ± 0.822	−24.16 ± 1.471		
$\Sigma^*\Sigma_c$	3791.64 ± 1.017	3759.45 ± 0.640	−32.19 ± 1.201		
$\Sigma^*\Sigma_c^*$	3823.67 ± 1.017	3798.47 ± 0.653	−25.20 ± 1.208		

For the $I = 0$, $S = -3$ system, the energies of different channels are shown in Table 5. We observe that no bound states are formed in these channels. All single-channel calculation results lie above their theoretical thresholds, respectively. After performing coupled-channel calculations, the system ground-state energy 3801.09 ± 0.834 MeV remains above the minimum threshold 3798.06 ± 1.302 MeV ($\Xi\Xi_c$), again indicating that no bound states exist. The results are physically reasonable, as clearly demonstrated in Figure 2. The effective attraction in these five channels ($\Lambda\Omega_c^*$, $\Xi\Xi_c$, $\Xi\Xi_c^*$, $\Xi^*\Xi_c'$, and $\Xi^*\Xi_c^*$) is insufficient to form any bound states, while the remaining channels exhibit purely repulsive effective potentials.

Table 5. The energy (in MeV) of different channels of the singly charmed dibaryons with $I = 0$, $S = -3$.

Channels	E_{th}	E_{sc}	B_{sc}	E_{cc}	B_{cc}
$\Lambda\Omega_c$	3800.46 ± 1.250	3808.17 ± 0.786	ub	3801.09 ± 0.834	ub
$\Lambda\Omega_c^*$	3817.95 ± 1.250	3857.99 ± 0.751	ub		
$\Lambda_c\Omega$	3887.06 ± 0.849	3893.80 ± 0.386	ub		
$\Xi\Xi_c$	3798.06 ± 1.302	3801.09 ± 0.834	ub		
$\Xi\Xi_c'$	3892.61 ± 1.167	3899.32 ± 0.703	ub		
$\Xi\Xi_c^*$	3917.52 ± 1.166	3921.04 ± 0.709	ub		
$\Xi^*\Xi_c$	3964.75 ± 0.963	3971.04 ± 0.635	ub		
$\Xi^*\Xi_c^*$	4084.21 ± 0.963	4089.45 ± 0.506	ub		
$\Xi^*\Xi_c'$	4059.30 ± 0.964	4061.86 ± 0.503	ub		

For the $I = 0$, $S = -5$ system, the energies of different channels are shown in Table 6. We observe that all single-channel energies remain above their theoretical thresholds, respectively. Coupled-channel calculations further demonstrate that the system ground-state energy of 4362.77 ± 1.133 MeV exceeds the lowest 4358.59 ± 0.464 MeV threshold ($\Omega\Omega_c$), confirming the absence of bound states even with channel coupling effects.

Table 6. The energy (in MeV) of different channels of the singly charmed dibaryons with $I = 0$, $S = -5$.

Channels	E_{th}	E_{sc}	B_{sc}	E_{cc}	B_{cc}
$\Omega\Omega_c$	4358.59 ± 0.464	4364.18 ± 1.016	ub	4362.77 ± 1.133	ub
$\Omega\Omega_c^*$	4376.08 ± 0.464	4381.11 ± 1.134	ub		

For the $I = \frac{1}{2}$, $S = 0$ system, the energies of different channels are shown in Table 7. We observe that, among these four channels, only the $\Sigma_c\Delta$ and $\Sigma_c^*\Delta$ channels form bound states, with binding energies of −23.83 ± 1.019 MeV and -43.61 ± 1.060 MeV, respectively.

The other two channels exhibit energies above their theoretical thresholds. Consequently, no bound states exist, which is fully consistent with our analysis of the effective potentials. After performing four-channel coupling calculations, the total energy of 3353.24 ± 0.849 MeV remains above the lowest single-channel threshold of 3349.50 ± 1.317 MeV ($N\Sigma_c$); no bound states below the lowest threshold exist in this system. However, after these channels couple, they may become resonance states, with the corresponding decay channels being $N\Sigma_c$ and $N\Sigma_c^*$. To investigate whether or not these states are resonance states, we will continue to study the scattering phase shifts of the open channels in the future.

Table 7. The energy (in MeV) of different channels of the singly charmed dibaryons with $I = \frac{1}{2}$, $S = 0$.

Channels	E_{th}	E_{sc}	B_{sc}	E_{cc}	B_{cc}
$N\Sigma_c$	3349.50 ± 1.317	3353.24 ± 0.849	ub		
$N\Sigma_c^*$	3381.74 ± 1.317	3392.19 ± 0.853	ub	3353.24 ± 0.849	ub
$\Sigma_c\Delta$	3670.83 ± 0.903	3647.01 ± 0.474	−23.83 ± 1.019		
$\Sigma_c^*\Delta$	3703.07 ± 0.903	3659.46 ± 0.556	−43.61 ± 1.060		

For the $I = \frac{1}{2}$, $S = -2$ system, the energies of different channels are shown in Table 8. The tabulated results demonstrate that all single-channel ground-state energies exceed their theoretical thresholds, respectively. Even after accounting for channel coupling effects, the system's lowest energy level of 3663.83 ± 0.955 MeV remains above the minimum single-channel threshold of 3661.74 ± 1.412 MeV ($\Sigma\Xi_c$). Therefore, we conclusively rule out the existence of bound states in this channel.

Table 8. The energy (in MeV) of different channels of the singly charmed dibaryons with $I = \frac{1}{2}$, $S = -2$.

Channels	E_{th}	E_{sc}	B_{sc}	E_{cc}	B_{cc}
$\Sigma_c\Xi$	3761.06 ± 1.110	3763.79 ± 0.651	ub		
$\Sigma\Xi_c$	3661.74 ± 1.412	3664.94 ± 0.956	ub		
$\Sigma\Xi_c'$	3756.29 ± 1.277	3760.88 ± 0.813	ub		
$\Sigma_c\Xi^*$	3927.75 ± 0.907	3931.17 ± 1.339	ub		
$\Sigma\Xi_c^*$	3781.20 ± 1.267	3788.38 ± 0.812	ub	3663.83 ± 0.955	ub
$\Xi\Sigma_c^*$	3793.30 ± 1.110	3796.45 ± 0.649	ub		
$\Xi_c\Sigma^*$	3828.43 ± 1.209	3833.93 ± 0.745	ub		
$\Xi_c'\Sigma^*$	3922.98 ± 1.074	3925.13 ± 0.614	ub		
$\Xi^*\Sigma_c^*$	3959.99 ± 0.907	3964.89 ± 0.444	ub		
$\Xi_c^*\Sigma^*$	3947.89 ± 1.073	3951.90 ± 0.616	ub		

For the $I = 1$, $S = -1$ system, the energies of different channels are shown in Table 9. Within this system, the single-channel calculations reveal that only the $\Sigma\Sigma_c$ forms a shallow bound state with a binding energy of −0.88 ± 1.438 MeV. All other single-channel energies lie above their theoretical thresholds, indicating the absence of bound states in these channels. Furthermore, our coupled-channel calculation energy is higher than the lowest threshold value ($N\Xi_c$). Therefore, we conclude that no bound states exist below the lowest threshold in this system. However, this state may decay into the $N\Xi_c$, $N\Xi_c'$, $\Lambda\Sigma_c$, $\Lambda_c\Sigma$, $\Lambda\Sigma_c^*$, $\Lambda_c\Sigma^*$, and $N\Xi_c^*$ channels and form a resonance. We will investigate this further by studying the open-channel scattering phase shifts.

For the $I = 1$, $S = -3$ system, the energies of different channels are shown in Table 10. All single-channel energies exceed their theoretical thresholds, demonstrating the absence of bound states in the single-channel approximation. After channel coupling, the computed energy, 3805.26 ± 1.173 MeV, is higher than the lowest threshold, 3798.06 ± 1.302 MeV ($\Xi\Xi_c$), confirming the absence of bound states in these channels. These numerical results align consistently with our effective potential analysis, demonstrating purely repulsive interactions in some channels, as shown in Figure 7, with the exception of the $\Xi_c'\Xi^*$ state.

Table 9. The energy (in MeV) of different channels of the singly charmed dibaryons with $I = 1$, $S = -1$.

Channels	E_{th}	E_{sc}	B_{sc}	E_{cc}	B_{cc}
$\Sigma\Sigma_c$	3624.74 ± 1.220	3623.86 ± 0.762	−0.88 ± 1.438		
$N\Xi_c$	3386.50 ± 1.509	3395.74 ± 1.045	ub		
$N\Xi_c'$	3481.05 ± 1.374	3489.93 ± 0.910	ub		
$\Lambda\Sigma_c$	3521.65 ± 1.352	3529.89 ± 0.896	ub		
$\Lambda_c\Sigma$	3432.02 ± 1.495	3441.02 ± 1.032	ub		
$\Lambda\Sigma_c^*$	3553.89 ± 1.352	3562.78 ± 0.896	ub		
$\Lambda_c\Sigma^*$	3598.71 ± 1.292	3607.14 ± 0.828	ub	3395.74 ± 1.045	ub
$N\Xi_c^*$	3505.96 ± 1.373	3515.30 ± 0.909	ub		
$\Xi_c\Delta$	3707.83 ± 1.095	3710.28 ± 0.635	ub		
$\Xi_c'\Delta$	3802.38 ± 0.960	3804.44 ± 0.504	ub		
$\Sigma\Sigma_c^*$	3656.98 ± 1.220	3661.94 ± 0.755	ub		
$\Sigma_c\Sigma^*$	3791.64 ± 1.017	3794.29 ± 0.553	ub		
$\Xi_c^*\Delta$	3827.29 ± 0.959	3829.58 ± 0.506	ub		
$\Sigma^*\Sigma_c^*$	3823.67 ± 1.017	3827.95 ± 0.553	ub		

Table 10. The energy (in MeV) of different channels of the singly charmed dibaryons with $I = 1$, $S = -3$.

Channels	E_{th}	E_{sc}	B_{sc}	E_{cc}	B_{cc}
$\Sigma\Omega_c$	3903.55 ± 1.110	3910.56 ± 0.647	ub		
$\Xi\Xi_c$	3798.06 ± 1.302	3805.30 ± 0.838	ub		
$\Sigma_c\Omega$	4079.78 ± 0.574	4085.53 ± 0.504	ub		
$\Sigma\Omega_c^*$	3921.04 ± 1.110	3928.33 ± 0.646	ub		
$\Xi_c'\Xi^*$	4059.30 ± 0.964	4063.89 ± 0.499	ub		
$\Xi_c\Xi^*$	3964.75 ± 1.099	3972.15 ± 0.636	ub	3805.26 ± 1.173	ub
$\Xi\Xi_c^*$	3917.52 ± 1.110	3924.83 ± 0.702	ub		
$\Sigma^*\Omega_c$	4070.24 ± 0.907	4076.09 ± 0.444	ub		
$\Sigma_c^*\Omega$	4112.02 ± 0.574	4118.34 ± 0.110	ub		
$\Sigma^*\Omega_c^*$	4087.73 ± 0.907	4093.79 ± 0.444	ub		
$\Xi^*\Xi_c^*$	4084.21 ± 0.963	4090.34 ± 0.499	ub		

For the $I = \frac{3}{2}$, $S = 0$ system, the energies of different channels are shown in Table 11. Within this system, single-channel calculations indicate that only the $\Sigma_c\Delta$ state forms a bound state with a binding energy of -3.11 ± 1.005 MeV. All other channels yield energies above their theoretical thresholds, respectively, confirming that no bound states exist in these channels. When channel coupling is considered, the system ground-state energy 3359.28 ± 0.853 MeV remains above the fundamental theoretical threshold 3349.50 ± 1.317 MeV $(N\Sigma_c)$. Therefore, we conclude that in this state there are no bound states below the lowest threshold. Yet, this state may decay into the $N\Sigma_c$, $N\Sigma_c^*$ channel, giving rise to a resonance. We will pursue this question through the scattering phase shifts in the open-channel analysis.

Table 11. The energy (in MeV) of different channels of the singly charmed dibaryons with $I = \frac{3}{2}$, $S = 0$.

Channels	E_{th}	E_{sc}	B_{sc}	E_{cc}	B_{cc}
$N\Sigma_c$	3349.50 ± 1.317	3359.29 ± 0.853	ub		
$N\Sigma_c^*$	3381.74 ± 1.317	3389.20 ± 0.850	ub	3359.28 ± 0.853	ub
$\Sigma_c\Delta$	3670.83 ± 0.903	3667.72 ± 0.443	−3.11 ± 1.005		
$\Sigma_c^*\Delta$	3703.07 ± 0.903	3707.86 ± 0.436	ub		

For the $I = \frac{3}{2}$, $S = -2$ system, the energies of different channels are shown in Table 12. The single-channel calculations for this state reveal that only the $\Xi^*\Sigma_c^*$ state constitutes a bound state with a binding energy of -5.57 ± 1.092 MeV. For all other states, the single-channel calculation results exceed their theoretical thresholds due to

the purely repulsive nature of their effective potentials, making bound-state formation unlikely. Furthermore, the channel coupling calculations demonstrate that the system's lowest energy level 3668.94 ± 0.948 MeV remains above the minimum theoretical threshold 3661.74 ± 1.412 MeV of the system ($\Sigma\Xi_c$). Hence, we find that, within this configuration, no bound states exist whose energies fall beneath the minimal threshold. Nevertheless, this state could potentially decay through the remaining seven channels, giving rise to resonance. We plan to examine this possibility through detailed analysis of open-channel scattering phase shifts in subsequent research.

Table 12. The energy (in MeV) of different channels of the singly charmed dibaryons with $I = \frac{3}{2}$, $S = -2$.

Channels	E_{th}	E_{sc}	B_{sc}	E_{cc}	B_{cc}
$\Sigma_c\Xi$	3761.06 ± 1.110	3768.49 ± 0.646	ub		
$\Sigma\Xi_c$	3661.74 ± 1.412	3669.34 ± 0.949	ub		
$\Sigma\Xi_c'$	3756.29 ± 1.277	3764.25 ± 0.813	ub		
$\Sigma_c\Xi^*$	3927.75 ± 0.907	3933.88 ± 0.442	ub		
$\Sigma\Xi_c^*$	3781.20 ± 1.267	3788.98 ± 0.812	ub	3668.94 ± 0.948	ub
$\Xi\Sigma_c^*$	3793.30 ± 1.110	3801.80 ± 0.646	ub		
$\Xi_c\Sigma^*$	3828.43 ± 1.209	3836.46 ± 0.745	ub		
$\Xi_c'\Sigma^*$	3922.98 ± 1.074	3928.37 ± 0.610	ub		
$\Xi^*\Sigma_c^*$	3959.99 ± 0.907	3954.42 ± 0.609	−5.57 ± 1.092		
$\Xi_c^*\Sigma^*$	3947.89 ± 1.073	3966.57 ± 0.442	ub		

For the $I = 2$, $S = -1$ system, the energies of different channels are shown in Table 13. In this state, all seven channels exhibit single-channel energies above their theoretical thresholds, which implies that no bound states are present in these channels. Coupled-channel calculations yield energies of 3633.55 ± 0.756 MeV, which exceed the system minimum threshold energy 3624.74 ± 1.220 MeV ($\Sigma\Sigma_c$), further confirming the absence of bound states. These results are fully consistent with the repulsive effective potentials presented in Figure 10.

Table 13. The energy (in MeV) of different channels of the singly charmed dibaryons with $I = 2$, $S = -1$.

Channels	E_{th}	E_{sc}	B_{sc}	E_{cc}	B_{cc}
$\Xi_c\Delta$	3707.83 ± 1.095	3716.40 ± 0.632	ub		
$\Xi_c'\Delta$	3802.38 ± 0.960	3808.93 ± 0.495	ub		
$\Sigma\Sigma_c^*$	3656.98 ± 1.220	3664.12 ± 0.754	ub		
$\Sigma_c\Sigma^*$	3791.43 ± 1.017	3797.31 ± 0.541	ub	3633.55 ± 0.756	ub
$\Sigma\Sigma_c$	3624.74 ± 1.220	3633.55 ± 0.756	ub		
$\Xi_c^*\Delta$	3827.29 ± 0.959	3834.01 ± 0.501	ub		
$\Sigma^*\Sigma_c^*$	3823.67 ± 1.017	3830.44 ± 0.551	ub		

For the $I = \frac{5}{2}$, $S = 0$ system, the energies of different channels are shown in Table 14. Table 14 clearly demonstrates that the single-channel energies of both channels exceed their theoretical thresholds, ruling out the possibility of bound states. Even after considering channel coupling effects, the system ground-state energy 3674.72 ± 0.434 MeV remains above the fundamental theoretical threshold 3670.83 ± 0.903 MeV ($\Sigma_c\Delta$), confirming the absence of bound states. This finding contradicts our initial assessment based on the effective potentials presented in Figure 11.

Table 14. The energy (in MeV) of different channels of the singly charmed dibaryons with $I = \frac{5}{2}$, $S = 0$.

Channels	E_{th}	E_{sc}	B_{sc}	E_{cc}	B_{cc}
$\Sigma_c\Delta$	3670.83 ± 0.903	3674.72 ± 0.434	ub	3674.72 ± 0.434	ub
$\Sigma_c^*\Delta$	3703.07 ± 0.903	3709.99 ± 0.437	ub		

4. Summary

In this work, we systematically investigate the existence of S-wave singly charmed dibaryon states within the framework of the chiral quark model. We begin by constructing dibaryon wave functions and then calculate the effective potentials to analyze the interactions between two baryons of the singly charmed dibaryon systems, which can provide preliminary indications of possible bound-state formation. To further verify the existence of bound states, we perform both single-channel and coupled-channel energy calculations.

From the results of the effective potentials for different systems, we find that, for attractive interactions, states with the same isospin exhibit weaker attraction as the number of strange quarks increases. For example, in the isospin $I = 0$ sector, the deepest attractive potential reaches about 100 MeV for the channel $\Sigma^*\Sigma_c$ with strangeness $S = -1$, while the deepest attraction is less than 10 MeV for the channel $\Omega\Omega_c$ with $S = -5$. We also find that, for the fixed number of strange quarks, the attraction strengthens as isospin decreases. For instance, for systems with $S = -1$, the deepest attractive potential reaches 100 MeV for the channel $\Sigma^*\Sigma_c$ with $I = 0$ but drops below 5 MeV for the channel $\Sigma_c\Sigma^*$ with $I = 2$. The patterns of these changes in effective potentials indicate that, for dibaryon systems with smaller isospin quantum numbers and fewer strangeness numbers, the attraction between the two baryons is stronger, potentially making them more likely to form bound states. Therefore, experiments could initially focus on searching for these states.

From the results of the bound-state calculation, we find that there is no bound state below the lowest threshold in the present systems. Nevertheless, single-channel bound states do appear, and each of them can decay via open channels. Their nature can be probed further through the scattering process of the open channels. All the potentially existing bound states are compiled in Table 15, together with their possible two-body decay channels. The results show that the interaction potentials of the $\Sigma\Sigma_c$, $\Sigma\Sigma_c^*$, $\Sigma^*\Sigma_c$, $\Sigma^*\Sigma_c^*$, $\Sigma_c\Delta$, and $\Sigma_c^*\Delta$ states are rather deep and strongly attractive, giving rise to a pronounced single-channel bound state. Such states are likely to appear as resonances, and they will therefore be primary targets in our future scattering analyses as well as worthwhile seeking states for experimental investigation.

Table 15. Quasi-stable states under distinct quantum numbers and their possible two-body decay channels.

I	S	Quasi-Stable States	Decay Channels
0	-1	$\Sigma\Sigma_c$ $\Sigma\Sigma_c^*$ $\Sigma^*\Sigma_c$ $\Sigma^*\Sigma_c^*$	$\Lambda\Lambda_c, N\Xi_c, N\Xi_c', N\Xi_c^*$
$\frac{1}{2}$	0	$\Sigma_c\Delta$ $\Sigma_c^*\Delta$	$N\Sigma_c$ $N\Sigma_c^*$
1	-1	$\Sigma\Sigma_c$	$N\Xi_c$ $N\Xi_c'$ $\Lambda\Sigma_c$ $\Lambda_c\Sigma$ $\Lambda\Sigma_c^*$ $\Lambda_c\Sigma^*$ $N\Xi_c^*$
$\frac{3}{2}$	0	$\Sigma_c\Delta$	$N\Sigma_c, N\Sigma_c^*$
$\frac{3}{2}$	-2	$\Xi^*\Sigma_c^*$	$\Sigma_c\Xi$ $\Sigma\Xi_c$ $\Sigma\Xi_c'$ $\Sigma_c\Xi^*$ $\Sigma\Xi_c^*$ $\Xi^*\Sigma_c^*$ $\Xi_c\Sigma^*$ $\Xi_c'\Sigma^*$ $\Xi_c^*\Sigma^*$

While this work has systematically investigated the existence of singly charmed dibaryon states, there remain several directions for future research. First, our current study has focused exclusively on bound states and has not addressed possible resonance states; studying the scattering process is necessary for confirming the existence of resonance states. Second, the present work only studies ground-state configurations; dibaryon systems with higher partial waves (P-waves, D-waves, etc.) are also worth studying. From the study of dibaryon systems composed of light quarks, it can be seen that the possible dibaryons are mainly in the ground state, such as d^*. Therefore, it is unknown whether dibaryons composed of heavy quarks exist in a highly excited state, and specific computational research is needed. However, for $S-$wave bound states, they can decay into $D-$wave open

channels, which will affect the decay width of the resonance states. Due to the fact that $S-$ and $D-$ waves are coupled through tensor forces, this effect will not be too significant, but it still needs to be judged through specific calculations, which is work that will be conducted in the future. Such extensions will provide a more complete understanding of the exotic hadron spectrum.

Author Contributions: Methodology, Y.C. and Z.T.; Software, Y.C. and J.T.; Resources, J.T.; Data curation, Y.D.; Writing—original draft, Y.D.; Writing—review editing, H.H.; Visualization, Z.T.; Supervision, H.H. and J.P.; Project administration, J.P. All authors have read and agreed to the published version of the manuscript.

Funding: This work was partly supported by the National Natural Science Foundation of China under Contract Nos. 12575088, 11675080, 11775118, and 11535005.

Data Availability Statement: The original contributions presented in this study are included in the article. Further inquiries can be directed to the corresponding authors.

Conflicts of Interest: The authors declare no conflicts of interest. The funders had no role in the design of the study; in the collection, analyses, or interpretation of data; in the writing of the manuscript; or in the decision to publish the results.

References

1. Urey, H.C.; Brickwedde, F.G.; Murphy, G.M. A Hydrogen Isotope of Mass 2. *Phys. Rev.* **1932**, *39*, 164–165. [CrossRef]
2. Jaffe, R.L. Perhaps a Stable Dihyperon. *Phys. Rev. Lett.* **1977**, *38*, 617. [CrossRef]
3. Kamae, T.; Fujita, T. Possible Existence of a Deeply Bound $\Delta\Delta$ System. *Phys. Rev. Lett.* **1977**, *38*, 471–475. [CrossRef]
4. Goldman, J.T.; Maltman, K.; Stephenson, G.J., Jr.; Schmidt, K.E.; Wang, F. An 'inevitable' nonstrange dibaryon. *Phys. Rev. C* **1989**, *51*, 1889–1895. [CrossRef]
5. Adlarson, P. et al. [WASA-at-COSY Collaboration] Isospin Decomposition of the Basic Double-Pionic Fusion in the Region of the ABC Effect. *Phys. Lett. B* **2013**, *721*, 229–236. [CrossRef]
6. Goldman, J.T.; Maltman, K.; Stephenson, G.J., Jr.; Schmidt, K.E.; Wang, F. strangeness-3 dibaryon. *Phys. Rev. Lett.* **1987**, *59*, 627. [CrossRef] [PubMed]
7. Oka, M. Flavor-octet dibaryons in the quark model. *Phys. Rev. D* **1988**, *38*, 298. [CrossRef] [PubMed]
8. Silvestre-Brac, B.; Leandri, J. Systematics of q^6 systems in a simple chromomagnetic model. *Phys. Rev. D* **1992**, *45*, 4221. [CrossRef]
9. Dai, L.R.; Zhang, D.; Li, C.R.; Tong, L. Structures of $N\Omega$ and $\Delta\Omega$ Dibaryons. *Chin. Phys. Lett.* **2007**, *24*, 389.
10. Li, Q.B.; Shen, P.N. $N\Omega$ and $\Delta\Omega$ dibaryons in $SU(3)$ chiral quark model. *Eur. Phys. J. A* **2000**, *8*, 417–421. [CrossRef]
11. Huang, H.X.; Ping, J.L.; Wang, F. Further study of the $N\Omega$ dibaryon within constituent quark models. *Phys. Rev. C* **2015**, *92*, 065202. [CrossRef]
12. Chen, X.H.; Wang, Q.N.; Chen, W.; Chen, H.X. Mass spectra of $N\Omega$ dibaryons in the $^3S_1$ and $^5S_1$ channels. *Phys. Rev. D* **2021**, *103*, 094011. [CrossRef]
13. Adam, J. et al. [STAR Collaboration] The Proton-Ω correlation function in $Au + Au$ collisions at $\sqrt{s_{NN}} = 200$ GeV. *Phys. Lett. B* **2019**, *790*, 490–497. [CrossRef]
14. Collaboration, A. et al. [ALICE Collaboration] Unveiling the strong interaction among hadrons at the LHC. *Nature* **2020**, *588*, 232–238. [CrossRef]
15. Yan, Y.; Huang, Q.; Yang, Y.; Huang, H.X.; Ping, J.L. Investigating the p-Ω interactions and correlation functions. *Sci. China Phys. Mech. Astron.* **2025**, *68*, 232012. [CrossRef]
16. Aaij , R. et al. [LHCb Collaboration] Observation of the doubly charmed baryon Ξ_{cc} *Phys. Rev. Lett.* **2017**, *119*, 112001.
17. Lee, N.; Luo, Z.G.; Chen, X.L.; Zhu, S.L. Possible deuteron-like molecular states composed of heavy baryons. *Phys. Rev. D* **2011**, *84*, 014031. [CrossRef]
18. Liu, Y.R.; Oka, M. $\Lambda_c\Omega$ bound states revisited. *Phys. Rev. D* **2012**, *85*, 014015. [CrossRef]
19. Meng, L.; Li, N.; Zhu, S.L. Deuteron-like states composed of two doubly charmed baryons. *Phys. Rev. D* **2017**, *95*, 114019. [CrossRef]
20. Chen, R.; Wang, F.L.; Hosaka, A.; Liu, X. Exotic triple-charm deuteronlike hexaquarks. *Phys. Rev. D* **2018**, *97*, 114011. [CrossRef]
21. Pan, Y.W.; Liu, M.Z. Triply charmed dibaryons in the one-boson exchange model. *Phys. Rev. D* **2020**, *102*, 054025. [CrossRef]
22. Wang, Z.G. Triply-charmed dibaryon states or two-baryon scattering states from QCD sum rules. *Phys. Rev. D* **2020**, *102*, 034008. [CrossRef]
23. Junnarkar, P.M.; Mathur, N. Study of three-flavored heavy dibaryons using lattice QCD. *Phys. Rev. D* **2022**, *106*, 054511. [CrossRef]

24. Lyu, Y.; Tong, H.; Sugiura, T.; Aoki, S.; Doi, T.; Hatsuda, T.; Meng, J.; Miyamoto, T. Dibaryon with Highest Charm Number near Unitarity from Lattice QCD. *Phys. Rev. Lett.* **2021**, *127*, 072003. [CrossRef]
25. Junnarkar, P.M.; Mathur, N. Spectrum of two-flavored spin-zero heavy dibaryons in lattice QCD. *Phys. Rev. D* **2025**, *111*, 014512. [CrossRef]
26. Gal, A.; Garcilazo, H.; Valcarce, A.; Fernández-Caramés, T. Pion-assisted charmed dibaryon candidate. *Phys. Rev. D* **2014**, *90*, 014019. [CrossRef]
27. Richard, J.M.; Valcarce, A.; Vijande, J. Very Heavy Flavored Dibaryons. *Phys. Rev. Lett.* **2020**, *124*, 212001. [CrossRef]
28. Xia, Z.C.; Fan, S.J.; Zhu, X.M.; Huang, H.X.; Ping, J.L. Search for doubly heavy dibaryons in the quark delocalization color screening model. *Phys. Rev. C* **2022**, *105*, 025201. [CrossRef]
29. Martín-Higueras, P.; Entem, D.R.; Ortega, P.G.; Segovia, J.; Fernández, F. Study of the $\Omega_{ccc}\Omega_{ccc}$ and $\Omega_{bbb}\Omega_{bbb}$ dibaryons in constituent quark model. *arXiv* **2024**, arXiv:2406.19208. [CrossRef]
30. Cui, Y.; Wu, Y.H.; Huang, H.X.; Ping, J.L.; Zhu, X.M. Search for singly charmed dibaryons in baryon-baryon scattering. *Phys. Rev. D* **2024**, *110*, 114055. [CrossRef]
31. Valcarce, A.; Garcilazo, H.; Fernandez, F.; Gonzalez, P. Quark-model study of few-baryon systems. *Rep. Prog. Phys.* **2005**, *68*, 965–1042. [CrossRef]
32. Vijande, J.; Fernandez, F.; Valcarce, A. Constituent quark model study of the meson spectra. *J. Phys. G* **2005**, *31*, 481. [CrossRef]
33. Beringer, J. et al. [Particle Data Group] Review of Particle Physics. *Phys. Rev. D* **2012**, *86*, 010001. [CrossRef]
34. Kamimura, M. Chapter V. A Coupled Channel Variational Method for Microscopic Study of Reactions between Complex Nuclei. *Prog. Theor. Phys. Suppl.* **1977**, *62*, 236–294. [CrossRef]
35. Bali, G.S. QCD forces and heavy quark bound states. *Phys. Rep.* **2001**, *343*, 1–136. [CrossRef]